

Expected intermediate mass black holes in the Virgo cluster. II. Late-type galaxies

Alister W. Graham¹★, Roberto Soria^{2,3,4}, and Benjamin L. Davis¹

¹Centre for Astrophysics and Supercomputing, Swinburne University of Technology, Hawthorn, VIC 3122, Australia.

²College of Astronomy and Space Sciences, University of the Chinese Academy of Sciences, Beijing 100049, China

³International Centre for Radio Astronomy Research, Curtin University, GPO Box U1987, Perth, WA 6845, Australia.

⁴Sydney Institute for Astronomy, School of Physics A28, The University of Sydney, Sydney, NSW 2006, Australia.

Accepted XXX. Received YYY; in original form ZZZ

ABSTRACT

The *Chandra X-ray Observatory*’s Cycle 18 Large Program titled ‘Spiral galaxies of the Virgo Cluster’ will image 52 galaxies with the ACIS-S detector. Combined with archival data for an additional 22 galaxies, this will represent the complete sample of 74 spiral galaxies in the Virgo cluster with star-formation rates $\geq 0.3 M_{\odot} \text{ yr}^{-1}$. Many of these galaxies are expected to have an active nucleus, signalling the presence of a central black hole. In preparation for this survey, we predict the central black hole masses using the latest black hole scaling relations based on spiral arm pitch angle ϕ , velocity dispersion σ , and total stellar mass $M_{*,\text{galaxy}}$. With a focus on intermediate mass black holes ($10^2 < M_{\text{bh}}/M_{\odot} < 10^5$), we highlight NGC 4713 and NGC 4178, both with $M_{\text{bh}} \approx 10^3\text{--}10^4$ (an estimate which is further supported in NGC 4178 by its nuclear star cluster mass). From *Chandra* archival data, we find that both galaxies have a point-like nuclear X-ray source, with unabsorbed 0.3–10 keV luminosities of a few times $10^{38} \text{ erg s}^{-1}$. In NGC 4178, the nuclear source has a soft, probably thermal, spectrum consistent with a stellar-mass black hole in the high/soft state, while no strong constraints can be derived for the nuclear emission of NGC 4713. In total, 33 of the 74 galaxies are predicted to have $M_{\text{bh}} < (10^5\text{--}10^6) M_{\odot}$, and several are consistently predicted, via three methods, to have masses of $10^4\text{--}10^5 M_{\odot}$, such as IC 3392, NGC 4294 and NGC 4413. We speculate that a sizeable population of IMBHs may reside in late-type spiral galaxies with low stellar mass ($M_{*} \lesssim 10^{10} M_{\odot}$).

Key words: black hole physics – X-rays: galaxies – (galaxies:) quasars: supermassive black holes – galaxies: spiral – galaxies: structure – galaxies: individual: IC 3392, NGC 4178, NGC 4294, NGC 4413, NGC 4470, NGC 4713

1 INTRODUCTION

In the young universe, massive metal-free Population III stars (Schwarzschild & Spitzer 1953; Larson 1998) may have spawned ‘intermediate mass black holes’ (IMBHs) with masses greater than $10^2 M_{\odot}$ (e.g. Bond et al. 1984; Carr et al. 1984; Madau & Rees 2001; Schneider et al. 2002), but see Umeda & Nomoto (2003) and Fraser et al. (2017) who cap the ‘Pop III’ masses at 120–130 M_{\odot} . Additional mechanisms have also been proposed for the creation of IMBHs (see, e.g., Miller & Colbert 2004 and Mezcua 2017), including: the runaway merging of stellar mass black holes and stars (Zel’dovich & Podurets 1965; Larson 1970; Shapiro & Teukolsky 1985; Quinlan & Shapiro 1990; Portegies Zwart & McMillan 2002; Gürkan et al. 2004); primordial black holes (e.g. Argyres et al. 1998; Bean & Magueijo 2002; Carr et al. 2010; Grobov et al. 2011);

the direct collapse of massive gas clouds, bypassing the Pop III stage (Doroshkevich et al. 1967; Umemure et al. 1993; Bromm & Loeb 2003; Mayer et al. 2010); and a stunted or inefficient growth of nuclear black holes via gas accretion at the centres of galaxies (e.g. Johnson & Bromm 2007; Sijacki et al. 2007; Alvarez et al. 2009; Heckman & Best 2014). In the last of those alternative scenarios, IMBHs are an intermediate step on the way to the maturation of supermassive black holes (SMBHs, $M_{\text{bh}} > 10^5 M_{\odot}$; Rees 1984; Shankar et al. 2004; Ferrarese & Ford 2005; Kormendy & Ho 2013; Graham 2016a, and references therein).

In contrast to the plethora of theoretical formation models, direct observational detection of IMBHs remains elusive. There is a long history of disproved suggestions and claims of IMBHs in globular clusters, stretching back to at least the X-ray data from Clark et al. (1975). Most recently, the presence of an IMBH with a mass of $\approx 2000 M_{\odot}$ in the core of the Milky Way globular cluster 47 Tuc was suggested by a kinematic modelling of its pulsars (Kiziltan

★ E-mail: AGraham@swin.edu.au

et al. 2017), but there is no electromagnetic evidence for its existence, nor proof of any other IMBH in Galactic globular clusters (Anderson & van der Marel 2010; Strader et al. 2012).

In the centre of nearby galaxies, there are only a handful of candidate IMBHs with an X-ray detection, i.e. with plausible signature of gas accretion onto a compact object. These include: NGC 4178¹ (Satyapal et al. 2009; Secrest et al. 2012); LEDA 87300 (Baldassare et al. 2015; Graham et al. 2016); NGC 404 (Nguyen et al. 2017); NGC 3319 (Jiang et al. 2018); and possibly NGC 4395 (Iwasawa et al. 2000; Shih et al. 2003; Filippenko & Ho 2003, Nucita et al. 2017, but see den Brok et al. 2015).

Outside of galactic nuclei, IMBH searches initially focused on a rare class of point-like X-ray sources with X-ray luminosities $\sim 10^{40}$ – 10^{41} erg s⁻¹ (e.g. Colbert & Mushotzky 1999; Swartz et al. 2008; Sutton et al. 2012; Mezcua et al. 2015; Zolotukhin et al. 2016). This was partly based on the assumption that the X-ray luminosity of an accreting compact object cannot be much in excess of its classical Eddington limit (hence, luminosities $\gtrsim 10^{40}$ erg s⁻¹ would require BH masses $\gtrsim 100 M_\odot$), and partly on the detection of a low-temperature thermal component ($kT \sim 0.2$ keV) that was interpreted as emission from an IMBH accretion disk (Miller et al. 2003). However, most of the sources in this class are today interpreted as super-Eddington stellar-mass black holes or neutron stars (Feng & Soria 2011; Kaaret et al. 2017). To date, the most solid IMBH identification in this class of off-nuclear sources is HLX-1, in the galaxy cluster Abell 2877, and seen in projection near the S0 galaxy ESO 243-49 (Farrell et al. 2009, Soria et al. 2010; Yan et al. 2015; Webb et al. 2010, 2017). HLX-1 has a mass of $\sim 10^4 M_\odot$ (Davis et al. 2011; Godet et al. 2012; Soria et al. 2017) and may reside in the remnant nucleus of a gravitationally-captured and tidally-stripped satellite galaxy (Mapelli et al. 2013; Farrell et al. 2014), which leads us back to galactic nuclei as the most likely cradle of IMBHs.

In this work, we focus on IMBH candidates in galactic nuclei. Due to their low mass, it is currently impossible to spatially resolve the gravitational sphere-of-influence of these black holes; therefore, astronomers need to rely on alternative means to gauge their mass. There are now numerous galaxy parameters that can be used to predict the mass of a galaxy’s central black hole, and Koliopanos et al. (2017) report on the consistency of various black hole scaling relations.

The existence, or scarcity, of central IMBHs obviously has implications for theories regarding the growth of supermassive black holes. For example, some have theorised that supermassive black holes started from seed masses $\gtrsim 10^5 M_\odot$ — created from the direct collapse of large gas clouds and viscous high-density accretion-discs (e.g. Haehnelt & Rees 1993; Loeb & Rasio 1994; Koushiappas, Bullock & Dekel 2004; Regan et al. 2017) — which could potentially bypass the very existence of IMBHs. Therefore, defining the demography of IMBHs has implications for the co-evolution of massive black holes and their host galaxy alike.

For two reasons, spiral galaxies may represent a more promising field to plough than early-type galaxies or dwarf galaxies². This is due to their low mass bulges and disks — and thus low mass black holes — and the presence of gas which may result in an ac-

tive galactic nucleus around the central black hole, potentially betraying the black hole’s presence. Until very recently, the largest sample of spiral galaxies, with directly measured BH masses, that had been carefully decomposed into their various structural components, e.g. bar, bulge, rings, etc., and therefore with reliable bulge parameters, stood at 17 galaxies (Savorgnan & Graham 2016). This has now more than doubled, with a sample of 43 such spiral galaxies³ presented in Davis et al. (2018a), along with revised and notably more accurate $M_{\text{bh}}-M_{*,\text{bulge}}$ and $M_{\text{bh}}-M_{*,\text{galaxy}}$ relations for the spiral galaxies (Davis et al. 2018b).

Here, we apply three independent, updated, black hole scaling relations to a sample of 74 spiral galaxies in the Virgo cluster. X-ray images already exist for 22 members of this sample, and new images will be acquired for the remaining members during the *Chandra X-ray Observatory*’s Cycle 18 observing program (see Section 2). This paper’s tabulation of predicted black hole masses for these 74 galaxies will serve as a reference, enabling two key objectives to be met. First, in the pursuit of evidence for the (largely) missing population of IMBHs, we will eventually be able to say which of the 74 galaxies predicted to have an IMBH additionally contain electromagnetic evidence for the existence of a black hole. We are not, however, just laying the necessary groundwork for this, but we are able to now, and do, explore which of the initial 22 galaxies contain both an active galactic nucleus (AGN) and a predicted IMBH. Second, by combining the existing and upcoming X-ray data with the predicted black hole masses for the full sample, we will be able to compute the black holes’ Eddington ratios and investigate how the average Eddington-scaled X-ray luminosity scales with BH mass (Soria et al. 2018, in preparation). Gallo et al. (2010) have already attempted this measurement for the early-type galaxies in the Virgo cluster, and in Graham & Soria (2018, hereafter Paper I) we revisit this measurement using updated black hole scaling relations for early-type galaxies, such that in low-mass systems the black hole mass scales quadratically, rather than linearly, with the early-type galaxies’ B-band luminosity (Graham & Scott 2013).

The layout of this current paper is as follows. In Section (2) we briefly introduce the galaxy set that will be analysed. A more complete description will be provided in Soria et al. (2018, in preparation). In Section (3) we explain the measurements of pitch angle, velocity dispersion, and stellar mass that we have acquired for these 74 galaxies, and we introduce the latest (spiral galaxy) black hole scaling relations involving these quantities, from which we derive the expected black hole masses, that are presented in the Appendix. In Section (4) we compare the black hole mass predictions from the three independent methods. We additionally take the opportunity to combine the black hole scaling relations by eliminating the black hole mass term and providing revised galaxy scaling relations between pitch angle, velocity dispersion, and galaxy stellar mass. In Section (5) we pay particular attention to galaxies predicted to have black hole masses less than $10^5 M_\odot$, and we investigate the X-ray properties of those nuclei for which archival X-ray data already exists. Finally, Section (6) provides a discussion of various related issues.

¹ For NGC 4178, the prediction that $M_{\text{bh}} < 10^5 M_\odot$ is simply based on the assumption that the nuclear BH mass is less than 20 per cent of this galaxy’s nuclear star cluster mass.

² Given the rarity of dwarf spiral galaxies (Schombert et al. 1995; Graham et al. 2003), dwarf galaxies are overwhelmingly early-type galaxies.

³ With a central rather than global spiral pattern, we exclude the ES galaxy Cygnus A from the list of 44 galaxies in Davis et al. (2017), who, we note, reported that three of these remaining 43 galaxies appear to be bulgeless.

2 GALAXY SAMPLE

Soria et al. (2018, in preparation) selected the complete sample of 74 Virgo cluster spiral galaxies with star-formation rates $>0.3 M_{\odot} \text{ yr}^{-1}$ (see the Appendix for this galaxy list). This resulted in a mix of (early- and late-type) spiral galaxies, in the inner and outer regions of the cluster, spanning more than 5 mag in absolute B -band magnitude from roughly -18 to -23 mag (Vega). Of these 74 galaxies, just three have directly measured black hole masses; they are: NGC 4303, $\log(M_{\text{bh}}/M_{\odot}) = 6.58^{+0.07}_{-0.26}$ (Pastorini et al. 2007); NGC 4388, $\log(M_{\text{bh}}/M_{\odot}) = 6.90^{+0.04}_{-0.05}$ (Tadhunter et al. 2003); and NGC 4501, $\log(M_{\text{bh}}/M_{\odot}) = 7.13^{+0.08}_{-0.08}$ (Saglia et al. 2016).

In the X-ray bands, 22 of those galaxies already have archival *Chandra X-ray Observatory* data, and the rest are currently being observed with the Advanced CCD Imaging Spectrometer (ACIS-S) detector, as part of a 559-ks *Chandra* Large Project titled ‘Spiral galaxies of the Virgo cluster’ (PI: R. Soria. Proposal ID: 18620568). General results for our X-ray study, (including both nuclear and non-nuclear source catalogues, luminosity functions, multiband identifications, and comparisons between the X-ray properties as a function of Hubble type, will be presented in forthcoming work, once the observations have been completed. Here, we only use the archival *Chandra* data to characterise the nuclear X-ray properties of spiral galaxies that we identify as possible IMBH hosts, based on their black hole scaling relations.

3 PREDICTING BLACK HOLE MASSES

In this section, we introduce the three⁴ black hole scaling relations that will be used to predict the black hole masses of our Virgo cluster spiral galaxy sample, and we describe where the three associated parameter sets came from.

3.1 Pitch Angles

For galaxies whose disks are suitably inclined, such that their spiral pattern is visible, we project these images to a face-on orientation and measure their spiral arm ‘pitch angle’ ϕ , i.e. how tightly or loosely wound their spiral arms are. The mathematical description of the pitch angle, and the method of image analysis, is detailed in Davis et al. (2017), which also presents a significantly updated $M_{\text{bh}}-|\phi|$ relation (equation (1), below) for spiral galaxies, building on Seigar et al. (2008) and Berrier et al. (2013).

As noted in Davis et al. (2017), a prominent difficulty in pitch angle measurement is the identification of the fundamental pitch angle, which is analogous to the fundamental frequency in the musical harmonic series of frequencies. Pitched musical instruments produce musical notes with a characteristic timbre that is defined by the summation of a fundamental frequency and naturally occurring harmonics (integer multiples of the fundamental frequency). Careful Fourier analysis of the sound will allow discovery of the fundamental frequency and any perceptible harmonics. A synonymous scenario occurs in the measurement of galactic spiral arm pitch angle via two-dimensional Fourier analysis (Kalnajs 1975; Iye et al. 1982; Krakow et al. 1982; Puerari & Dottori 1992; Seigar

et al. 2005; Davis et al. 2012; Yu et al. 2018). Therefore, pitch angle measurement methods, when performed in haste, can incorrectly select a ‘harmonic’ pitch angle instead of the ‘fundamental’ pitch angle.

Similarly, the Fourier analysis of sound becomes less certain when the source tone is soft, short duration, or blended with contaminating noise. Spiral galaxies also become more difficult to analyse when resolution is poor, their disk orientation is close to edge-on, their spiral structure is intrinsically flocculent, or the arc length of their spiral segments are short. Whereas the former problems are stochastic and lead to increased uncertainty in pitch angle measurements (i.e., constant mean with an increased standard deviation), the latter problem of short spiral arc segments (i.e., small subtended polar angle) poses a potential systematic bias and can lead one to incorrectly identify a harmonic rather than the fundamental pitch angle. Typically, this problem manifests itself when spiral arc segments subtend polar angles $< \pi/2$ radians.

One clear benefit is that the measurement of galactic spiral arm pitch angle only requires simple imaging that highlights a perceptible spiral pattern, without the need of any photometric calibrations. Therefore, we accessed publicly available imaging from telescopes such as the Galaxy Evolution Explorer (GALEX), Hubble Space Telescope (HST), Spitzer Space Telescope (SST), Sloan Digital Sky Survey (SDSS), etc. This wide selection of telescopes also implies a wide range of passbands from far-ultraviolet up to mid-infrared wavelengths. Pour-Imani et al. (2016) concluded that pitch angle is statistically tighter in passbands that reveal young stellar populations, such as ultraviolet filters. The difference between young stellar spiral patterns and old stellar spiral patterns is small, typically less than 4 degrees in pitch angle. Because of this, we preferentially use young stellar passbands when they are available and if the resolution is sufficient to clearly display the spiral pattern. The same preference was applied in the derivation of the $M_{\text{bh}}-|\phi|$ relation in Davis et al. (2017).

The bisector linear regression between black hole mass and the absolute value of the spiral arm pitch angle, for the full sample of 44 ‘spiral’ galaxies⁵ with directly measured black hole masses, is such that

$$\log(M_{\text{bh}}/M_{\odot}) = (7.01 \pm 0.07) - (0.171 \pm 0.017)(|\phi| - 15^{\circ}), \quad (1)$$

with an intrinsic and total rms scatter in the $\log M_{\text{bh}}$ direction of 0.30 ± 0.08 and 0.43 dex, respectively (Davis et al. 2017, their equation 8).

Importantly, and curiously, the rms scatter in the $\log M_{\text{bh}}$ direction about this black hole scaling relation is smaller than the rms scatter observed in the other black hole scaling relations. This is in part due to the shallow slope of the relation in equation (1), and because of the careful pitch angle measurements that were determined using three different approaches (see Davis et al. 2017 for details). In passing, we note that the bulgeless galaxy NGC 2748 probably had an incorrect pitch angle assigned to it. Removing this galaxy, along with the early-type ES galaxy Cygnus A, plus two potential outliers (NGC 5055 and NGC 4395) seen in Davis et al. (2017, their figure 4), gives the revised and more robust relation

$$\log(M_{\text{bh}}/M_{\odot}) = (7.03 \pm 0.07) - (0.164 \pm 0.018)(|\phi| - 15^{\circ}), \quad (2)$$

with intrinsic and total rms scatter equal to 0.31 ± 0.07 and 0.41 dex,

⁴ There is also a scaling relation between M_{bh} and the bulge Sérsic index n (Graham & Driver 2007; Savorgnan 2016; Davis et al. 2018a). However, we do not use that relation for this work, partly because of the steepness at low masses, and partly to avoid the need for bulge/disk decompositions of our Virgo sample.

⁵ Davis et al. (2017) reported that excluding Cygnus A from the linear regression between black hole mass and spiral arm pitch angle did not have a significant effect.

respectively. Equation (2) has been used here to predict the black hole masses in 43 Virgo cluster spiral galaxies for which we were able to determine their pitch angle. The results are presented in the Appendix table.

3.2 Velocity Dispersions

Homogenised velocity dispersions are available in Hyperleda⁶ (Paturel et al. 2003) for 39 of the 74 Virgo galaxies. We have assigned a 15% uncertainty to each of these values.

The bisector linear regression between $\log M_{\text{bh}}$ and $\log \sigma$ — taken from Table 4 in Davis et al. (2017) for their reduced sample of 40 spiral galaxies (see below) — is given by

$$\log(M_{\text{bh}}/M_{\odot}) = (8.06 \pm 0.13) + (5.65 \pm 0.79) \log(\sigma/200 \text{ km s}^{-1}). \quad (3)$$

The intrinsic scatter is 0.51 ± 0.04 dex in the $\log M_{\text{bh}}$ direction, and the total rms scatter is 0.63 dex in the $\log M_{\text{bh}}$ direction. The slope of this expression agrees well with the $M_{\text{bh}}-\sigma$ relation from Savorgnan & Graham (2015, their Table 2), who found that their bisector regression yielded slopes between 4.8 and 5.7 for both ‘fast rotators’ and ‘slow rotators’. We have used equation (3) to predict the black hole masses for those 39 Virgo galaxies with available velocity dispersions, and we provide these values in the Appendix table.

As noted above, in deriving equation (3), four galaxies were excluded from the initial sample of 44 galaxies with directly measured black hole masses. NGC 6926 has no reported velocity dispersion, while Cygnus A is not a (typical) spiral galaxy, but rather an ES galaxy (see the discussion in Graham et al. 2016) with a nuclear, rather than large-scale, bar and spiral pattern. Another such example, albeit in a dwarf ES galaxy, is LEDA 2108986 (Graham et al. 2017). Finally, NGC 4395 and NGC 5055 are outliers that appear to have unusually low velocity dispersions; they were also excluded by Davis et al. (2017) in order to obtain a more robust regression unbiased by outliers.

3.3 Galaxy Stellar Masses

As revealed by the $M_{\text{bh}}-|\phi|$ relation in Davis et al. (2017, see also Seigar et al. 2008 and Ringermacher & Mead 2009), the central black hole masses in spiral galaxies are not unrelated to their disks. Furthermore, disks contain the bulk of the stellar mass in spiral galaxies.

We have derived total galaxy stellar masses for our sample of 74 Virgo cluster galaxies via the K' -band ($2.2 \mu\text{m}$) total apparent magnitudes (Vega) available in the GOLD Mine⁷ database (Gavazzi et al. 2003). We had initially explored using the *Two Micron All Sky Survey* (2MASS⁸, Jarrett et al. 2000) K_s -band total apparent magnitudes (Vega), but it sometimes under-estimates the galaxy luminosities (e.g., Kirby et al. 2008; Schombert 2011), as can be seen in Figure 1. The GOLD Mine apparent magnitudes were converted into absolute magnitudes using the mean, redshift-independent, distance moduli provided by the NASA/IPAC Extragalactic Database (NED)⁹. These absolute magnitudes were converted into solar units using an absolute magnitude for the Sun of

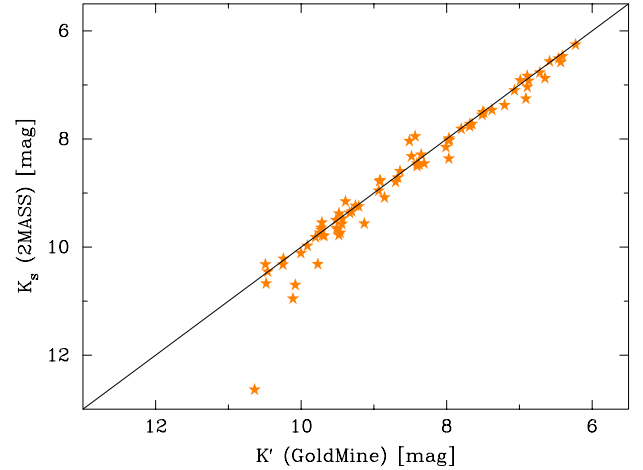


Figure 1. 2MASS K -band apparent magnitudes versus the K -band magnitudes from GOLD Mine. Both magnitudes have been corrected for Galactic extinction. At the faint end, some of the 2MASS magnitudes under-estimate the galaxy light.

$M_{\odot,K} = 3.28$ mag (Vega), taken from Willmer (2018), and then converted into a stellar mass, or rather a scaled-luminosity, using a constant K -band stellar mass-to-light ratio $M/L_K = 0.62$. The uncertainty that we have associated with our (GOLD Mine)-based stellar masses — which are tabulated in the Appendix — stems from adding in quadrature: (i) an assumed 10 per cent error on the apparent stellar luminosity, (ii) the standard deviation provided by NED for the mean redshift-independent distance modulus; and (iii) a 15 per cent error on the stellar mass-to-light ratio.

We have been able to verify these stellar masses by using, when available, the published $3.6\text{-}\mu\text{m}$ *Spitzer* galaxy magnitudes. Using the same redshift-independent distance moduli provided by NED¹⁰, Laine et al. (2014, their table 1) provide absolute galaxy magnitudes (AB, not Vega), at $3.6 \mu\text{m}$, for 31 of our 74 galaxies. On average, 25% of a spiral galaxy’s flux at $3.6 \mu\text{m}$ comes from the glow of dust (Querejeta et al. 2015, their Figures 8 and 9). We therefore dim Laine et al.’s magnitudes by 25% before converting them into stellar masses using $M_{\odot,3.6} = 6.02$ (AB mag) and a (stellar mass)-to-(stellar light) ratio $M/L_{3.6} = 0.60$ (Meidt et al. 2014)¹¹. This (stellar mass)-to-(stellar light) ratio, coupled with the above mentioned 25% flux reduction due to glowing dust, yields a (stellar mass)-to-(total light) ratio of 0.45, or $\log(M_*/L_{\text{tot}}) = -0.35$, which can be seen in Figure 10 of Querejeta et al. (2015) to provide a good approximation for more than 1600 large and bright nearby spiral galaxies. A comparison of these 31 *Spitzer*-based stellar masses with our (GOLD Mine)-based stellar masses can be seen in Figure (2). These masses are better thought of as scaled-luminosities, and we will return to this issue in the following subsection.

Using a symmetrical implementation¹² of the modified FITEXY routine (Press et al. 1992) from Tremaine et al. (2002), Davis et al. (2018b) reported a linear regression between black hole mass and galaxy stellar mass, for their sample of 40 spiral galaxies

¹⁰ We note that NGC 4276 only has one redshift-independent distance estimate; and we hereafter use the (Virgo + Great-Attractor + Shapley)-infall adjusted distance from NED for this galaxy.

¹¹ Based on a Chabrier (2003) initial stellar mass function.

¹² This involves taking the bisector of the ‘forward’ and ‘inverse’ regressions.

⁶ <http://leda.univ-lyon1.fr>

⁷ <http://goldmine.mib.infn.it/>

⁸ www.ipac.caltech.edu/2mass

⁹ <http://nedwww.ipac.caltech.edu>

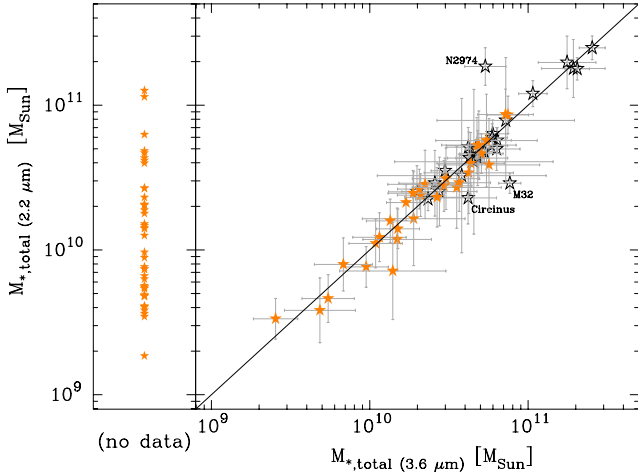


Figure 2. Galaxy stellar masses based on $2.2 \mu\text{m}$ magnitudes (with no dust correction), and using $M/L_K = 0.62$, versus the stellar masses based on the *Spitzer* $3.6 \mu\text{m}$ magnitudes (using a constant (stellar mass)-to-(total light) ratio $M_*/L_{\text{tot}} = 0.45$, from Querejeta et al. (2015). For the Virgo sample (orange stars), for which we used the GOLD Mine K -band data, 31 galaxies have *Spitzer* data. For the 43 galaxies (excluding the Milky Way) with directly measured black hole masses, we used the 2MASS K -band data (open black stars). The K -band data for NGC 2974 is likely contaminated by a foreground star.

with directly measured black hole masses (excluding the ES transition galaxy Cygnus A, and the three bulgeless galaxies NGC 4395, NGC 2748 and NGC 6926). The relation is

$$\log(M_{\text{bh}}/M_{\odot}) = (7.26 \pm 0.14) + (2.65 \pm 0.65) \log \left[M_{*,\text{galaxy}} / \nu(6.37 \times 10^{10} M_{\odot}) \right], \quad (4)$$

where ν (lowercase Υ) is a corrective stellar mass-to-light ratio term — which depends on the initial mass function of the stars and the star formation history — (see Davis et al. 2018a) that we can set equal to 1 given the agreement seen in Figure 2. The intrinsic scatter and total rms scatter in the $\log M_{\text{bh}}$ direction is equal to 0.64 and 0.75 dex, respectively. Equation (4) was used to predict the black hole masses for our 74 spiral galaxies, and the results are tabulated in the Appendix.

If the stellar mass is wrong by 50%, then the predicted logarithm of the black hole mass will be off by 0.47 dex. Combining this offset with the 1σ intrinsic scatter in equation (4), one could find that the predicted black hole mass is ~ 1 dex, i.e. an order of magnitude, different from the actual black hole mass. We therefore place less confidence in the black hole masses predicted from only the galaxy stellar mass. However, readers should be aware that our reported intrinsic and total rms scatters are not error-weighted quantities. That is, they can be dominated by outlying data points with large error bars, and therefore they can give a misleading view of how tightly defined the scaling relations are. The slope and intercept of the scaling relations presented here, and their associated uncertainty, do however take into account the error bars on the data used to define them.

Finally, Davis et al. (2018b) additionally reported the following steeper $M_{\text{bh}}-M_{*,\text{galaxy}}$ relation, derived using a sophisticated Bayesian analysis,

$$\log(M_{\text{bh}}/M_{\odot}) = (7.25^{+0.13}_{-0.14}) + (3.05^{+0.57}_{-0.49}) \log \left[M_{*,\text{galaxy}} / \nu(6.37 \times 10^{10} M_{\odot}) \right]. \quad (5)$$

This relation predicts black masses which agree well with those predicted from our $M_{\text{bh}}-\sigma$ relation (equation 3), but it tends to yield lower black hole masses than those predicted from our $M_{\text{bh}}-|\phi|$ relation (equation 1). This is also true for equation 4, and will be quantified in Section 4. Erring on the side of caution, such that we do not want to under-estimate the black hole masses and claim a greater population of IMBHs than actually exists, we proceed by using Equation (4) as our primary black hole mass based on the galaxy stellar mass. Black hole masses based on equation 5 are, however, additionally included.

3.3.1 What about colour-dependent M/L ratios?

We have assumed that the previous $M_{\text{bh}}-M_{*,\text{tot}}$ relations are log-linear, and we extrapolate this to masses below that which was used to define them. However, given that some of our Virgo cluster spiral galaxies are less massive and bluer than those in Davis et al. (2018b), it may be helpful if we provide some insight into what happens if the scaling which gives the scaled-luminosity, i.e. the so-called stellar mass, is not constant.

The 40 spiral galaxies used to define the above $M_{\text{bh}}-M_{*,\text{tot}}$ relations have stellar masses greater than $2 \times 10^{10} M_{\odot}$ (and absolute K -band magnitudes brighter than ≈ -23 mag), and, therefore, the assumption of a constant $3.6 \mu\text{m}$ M_*/L_* ratio of 0.60 (and M_*/L_{tot} ratio of 0.45) — which was used to derive the stellar masses in Davis et al. (2018b) — is likely to be a good approximation. This is because these galaxies’ stellar populations have roughly the same red colour. As such, the $M_{\text{bh}}-M_{*,\text{tot}}$ relations from Davis et al. (2018b) can be thought of as a (black hole)-(scaled luminosity) relation. Had the Davis et al. (2018b) sample contained some less massive *blue* galaxies, then, for the following reason, one may expect the M_{bh} -luminosity relation not to be log-linear, but to steepen at the faint end.

Bell & de Jong (2001) provide the following equation for the K -band (stellar mass)-to-(stellar light) ratio as a function of the $B-K$ optical-(near-infrared) colour:

$$\log M/L_K = 0.2119(B-K) - 0.9586. \quad (6)$$

We have obtained the 2MASS K -band data, and the RC3 B -band data¹³, for our Virgo spiral galaxies. Their $B-K$ colour, and the associated M/L_K ratio, is displayed in Figure 3. One can see that at $\mathfrak{M}_K \gtrsim -23$ mag, the M/L_K ratios become smaller. To maintain the log-linear $M_{\text{bh}}-M_{*,\text{tot}}$ relation (equation 4), obviously the M_{bh} -luminosity relation needs to steepen for $\mathfrak{M}_K \gtrsim -23$ mag. If we were to employ the falling M/L_K ratios seen in Figure 3 as one progresses to fainter galaxies, then we would also need to employ this steeper $M_{\text{bh}}-M_{*,\text{tot}}$ relation at these magnitudes. The net effect would be to cancel out and return one to the single log-linear $M_{\text{bh}}-M_{*,\text{tot}}$ relation (equation 4) that we are using together with a constant $M/L_K = 0.62$ for the GOLD Mine K -band data.

There is one additional element worthy of some exploration, and it pertains to the ν term seen in equations 4 and 5. We have made use of the SDSS Data Release 12 (Alam et al. 2015) to obtain three additional stellar mass estimates. Taylor et al. (2011) advocated that a $(g' - i')$ -dependent i' -band stellar mass-to-light ratio, $M_*/L_{i'}$, yields reliable stellar masses. Their relation is such that

¹³ The (Vega) B -band magnitudes are the B_T values from the *Third Reference Catalogue of Bright Galaxies* (de Vaucouleurs et al. 1991) as tabulated in NED, and were subsequently corrected for Galactic extinction using the values from Schlafly & Finkbeiner 2011, also tabulated in NED.

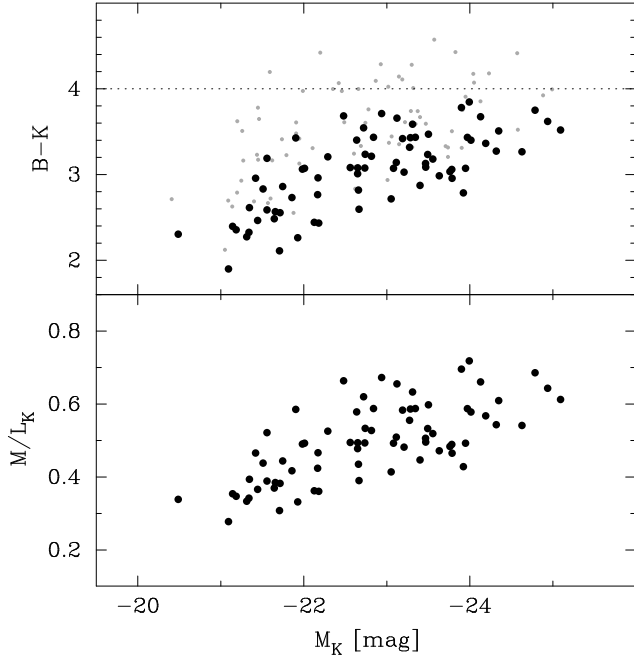


Figure 3. (RC3 B -band) - (Gold Mine K' -band) colour, and the $(B - K')$ -dependent K' -band stellar mass-to-light ratio (equation 6), versus the K' -band absolute magnitude. The grey points in the upper panel are based on the observed magnitudes, while the black points have been corrected for dust/inclination dimming using the prescription in Driver et al. (2008).

$\log(M_*/L_{i'}) = 0.70(g' - i') - 0.68$, and applies to the observed, i.e. not the dust-corrected, magnitudes. We have also used the relation $\log(M_*/L_{i'}) = 0.518(g' - i') - 0.152$ from Bell et al. (2003). Reddening due to dust will roughly move galaxies along this relation (see Figure 6 in Bell et al. 2003, and Figure 13 in Driver et al. 2007), and thus the relation can be applied to either the dust-corrected or observed magnitudes; for consistency with Taylor et al. (2011), we have chosen the latter. Finally, based on the stellar population synthesis model of Conroy et al. (2009), Roediger & Courteau (2015) give the relation $\log(M_*/L_{i'}) = 0.979(g' - i') - 0.831$. These three relations for the mass-to-light ratios have given us three more sets of stellar mass estimates for (most of) our 74 spiral galaxies, which are shown in Figure 4 against the (GOLD Mine K')-based mass estimates. While small random differences are apparent, due to uncertainties in the magnitudes and simplicities in the stellar population models, the main offsets that are visible can be captured / expressed by the ν term.

4 RESULTS

4.1 Pitch Angle vs Velocity Dispersion

Combining equations (1) and (3) to eliminate M_{bh} , one obtains the relation

$$\log(\sigma/200 \text{ km s}^{-1}) = 0.268 - 0.030|\phi|. \quad (7)$$

This is shown by the line in Figure (5), which plots $|\phi|$ versus $\log \sigma$ for spiral galaxies with directly measured black hole masses, plus our sample of Virgo cluster spiral galaxies, NGC 4395 and LEDA 87300.

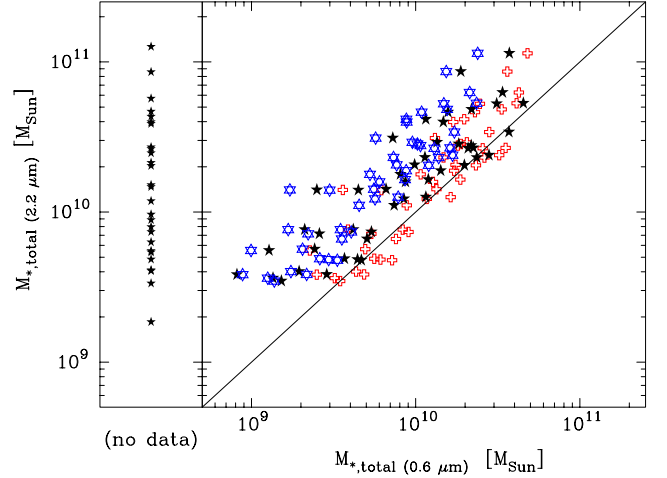


Figure 4. Stellar masses based on the GOLD Mine $2.2\text{-}\mu\text{m}$ K' -band magnitudes (not dust corrected, and using $M/L_K = 0.62$) versus the stellar masses based on the observed (not dust corrected) SDSS i' -band $0.62\text{-}\mu\text{m}$ magnitudes (using a $[g' - i']$ -dependent $M_*/L_{i'}$ ratio) from Bell et al. (2003, red crosses), Taylor et al. (2011, open blue hexagram), and Roediger & Courteau (2015, black filled stars). The data reveal the need for the ν term in equations 4 and 5.

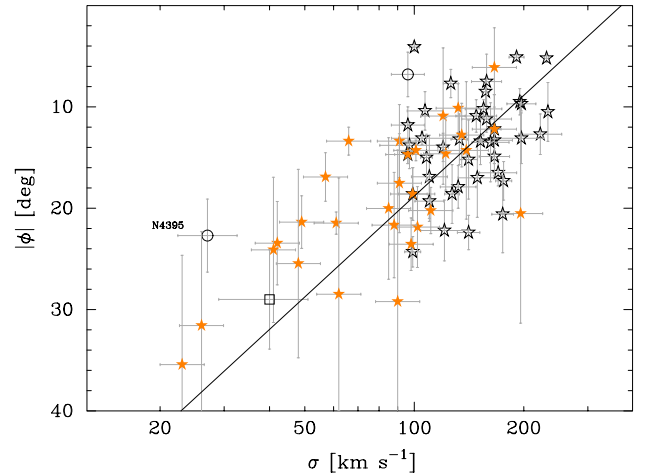


Figure 5. Absolute value of the spiral arm pitch angle, $|\phi|$, versus the stellar velocity dispersion σ . The open black stars (and circles) represent spiral galaxies with bulges (and without bulges) that have directly measured black hole masses (see Davis et al. 2017). The line represents equation (7), and is the expected trend based on the $M_{\text{bh}}-|\phi|$ relation given in equation (1) and the $M_{\text{bh}}-\sigma$ relation given in equation (3) for galaxies with directly measured black hole masses. The filled orange stars are the Virgo cluster spiral galaxies studied in this work. They appear to follow the line well, as does LEDA 87300 (open square).

The Virgo galaxies appear consistent with the trend (equation (7)) defined by the galaxy sample with directly measured black hole masses. Using equations (1) and (3) to predict the black hole masses in these Virgo galaxies, we plot the results in Figure (6). Of particular interest are NGC 4178 (Secrest et al. 2012) and NGC 4713, the two galaxies in the lower left of the right hand panel, plus NGC 4294 in the lower section of the left hand panel. They are predicted here to have black hole masses of 10^3 to $10^4 M_\odot$ (see the Appendix for every galaxies' predicted BH mass).

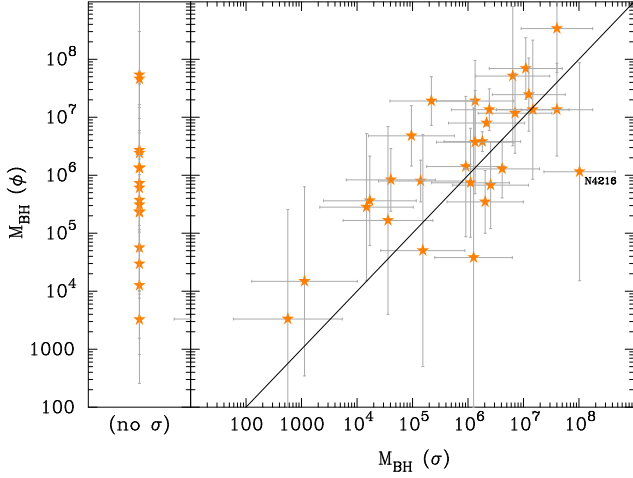


Figure 6. The predicted black hole masses in our Virgo galaxy sample, derived from, when available, the absolute value of the pitch angle $|\phi|$ (using equation (1)) and the velocity dispersion σ (using equation (3)).

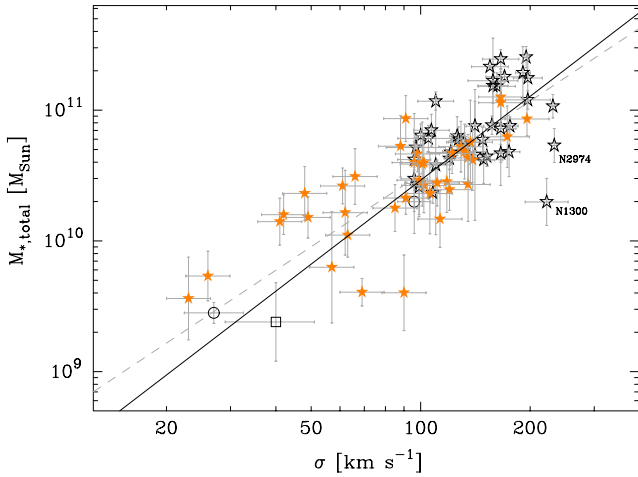


Figure 7. Galaxy stellar mass versus stellar velocity dispersion. Note: neither LEDA 87300 (open square) nor NGC 4395 (lower left open circle) were used in either the linear regression between M_{bh} and σ , nor between M_{bh} and $M_{*,\text{galaxy}}$, for the galaxy set with directly measured black hole masses (open stars and circles). Those regressions (equations (3) and (4), respectively), have been combined to produce equation (8) which is shown here by the solid line which has a slope of 2.13. The bulk of the Virgo cluster spiral galaxies (filled orange stars) appear to follow this line well. Equation 9, constructed from equation 3 and equation 5, is shown by the dashed grey line and has a slope equal to 1.85.

4.2 Stellar Mass vs Velocity Dispersion

Combining equations (3) and (4) to eliminate M_{bh} , one obtains the relation

$$\log(M_{*,\text{galaxy}}/6.37 \times 10^{10} M_{\odot}) = 0.302 + 2.132 \log(\sigma/200 \text{ km s}^{-1}). \quad (8)$$

This is shown by the solid line in Figure (7), which is a plot of $M_{*,\text{galaxy}}$ versus $\log \sigma$ for spiral galaxies with directly measured black hole masses, and for our sample of Virgo cluster spiral galaxies.

In Figure (8), we display the result of using equations (3) and

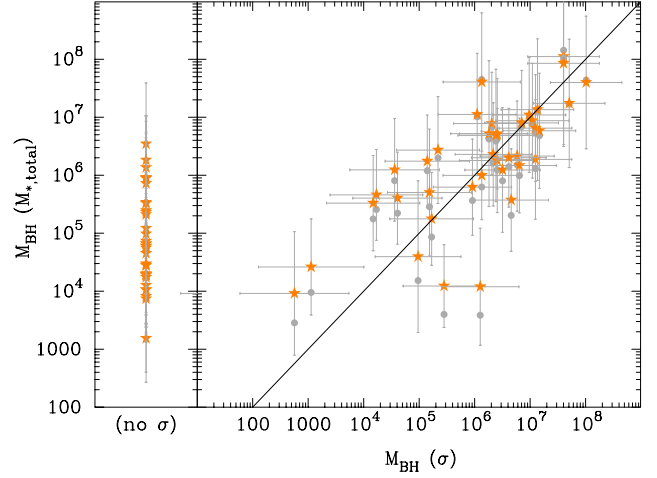


Figure 8. The orange stars show the predicted black hole masses in our Virgo galaxy sample, derived from, when available, the galaxy's stellar mass $M_{*,\text{galaxy}}$ (using equation (4)) and the stellar velocity dispersion σ (using equation (3)). The grey circles had their $(M_{*,\text{total}})$ -based black hole masses derived using equation 5.

(4) to predict the black hole masses in our Virgo galaxy sample. As before, two galaxies stand out, they are NGC 4178 and NGC 4713, the two galaxies in the lower left of the right hand panel of Figure (8). In addition, we note NGC 4396 and NGC 4299 in the lower section of the left hand panel of Figure (8)

Coupling equation 5, rather than equation 4, with equation 3 results in the relation

$$\log(M_{*,\text{galaxy}}/6.37 \times 10^{10} M_{\odot}) = 0.266 + 1.852 \log(\sigma/200 \text{ km s}^{-1}). \quad (9)$$

This equation is represented by the dashed grey line in Figure 7. Equation 8 and 9 give the scaling relation $M_{*,\text{galaxy}} \propto \sigma^{2 \pm 0.15}$ for spiral galaxies, which matches well with the relation for dwarf and ordinary early-type galaxies fainter than $M_B \approx -20.5$ mag (e.g. Davies et al. 1983; Matković & Guzmán 2005).

4.3 Pitch Angle vs Stellar Mass

Combining equations (1) and (4) to eliminate M_{bh} , one obtains the relation

$$\log(M_{*,\text{galaxy}}/6.37 \times 10^{10} M_{\odot}) = 0.874 - 0.0645|\phi|, \quad (10)$$

which is shown by the solid line in Figure (9). This is, once again, the expected relation for spiral galaxies with directly measured black hole masses. The trend seen here bears a resemblance to the distribution of spiral galaxies in the diagram of pitch angle versus B -band absolute magnitude shown by Kennicutt (1981, his figure 9).

Figure (10) displays the result of using equations (1) and (4) to predict the black hole masses in the Virgo spiral galaxies. This time there are many galaxies of interest in regard to potentially harbouring an IMBH. These findings have briefly been summarised in Table 1. Results for all galaxies are shown in the Appendix.

Finally, use of equation 5, rather than equation 4, results in the relation

$$\log(M_{*,\text{galaxy}}/6.37 \times 10^{10} M_{\odot}) = 0.762 - 0.0561|\phi|. \quad (11)$$

It is represented by the dashed grey line in Figure 9.

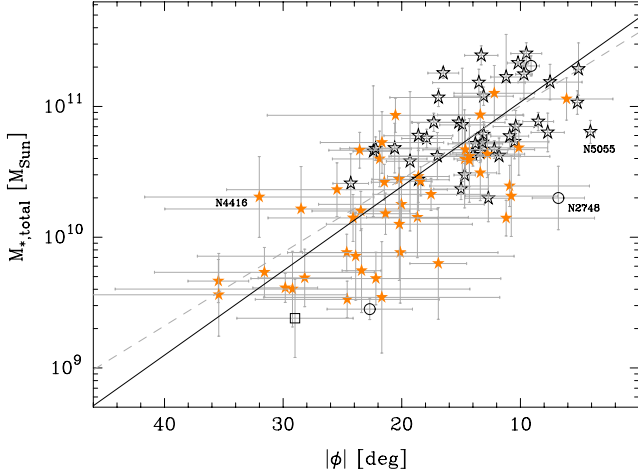


Figure 9. Galaxy stellar mass versus the absolute value of the spiral arm pitch angle. Symbols have the same meaning as in Figure (5). The solid line represents equation (10), and is the expected trend based on the $M_{\text{bh}}-|\phi|$ relation given in equation (1) and the $M_{\text{bh}}-M_{*,\text{galaxy}}$ relation given in equation (4), defined by galaxies with directly measured black hole masses (which excludes LEDA 87300, denoted by the open square). The dashed grey line is given by equation 11 and was obtained by combining equation 1 and equation 5.

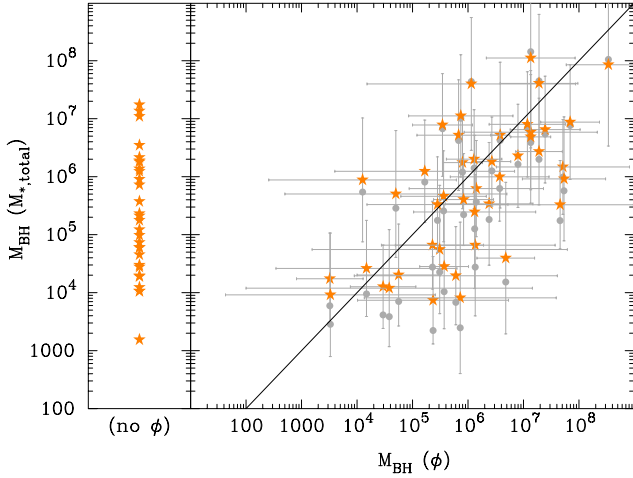


Figure 10. The orange stars show the predicted black hole masses in our Virgo galaxy sample, derived from both the galaxy's stellar mass $M_{*,\text{galaxy}}$ (using equation (4)) and, when available, the spiral arm pitch angle $|\phi|$ (using equation (1)). The grey circles show the $(M_{*,\text{total}})$ -based black hole masses derived using equation 5.

5 IMBH TARGETS OF INTEREST

From the previous section, we can identify five primary targets of interest: NGC 4178 and NGC 4713 (with three black hole mass estimates less than $10^5 M_\odot$), and IC 3392, NGC 4294 and NGC 4413 (with two black hole mass estimates less than $10^5 M_\odot$ but no velocity dispersion to provide a third black hole mass estimate). Table 1 lists these 5 galaxies along with an additional 28 galaxies which may have a central black hole mass of less than $10^5-10^6 M_\odot$.

The next step is to determine which of the candidate IMBH hosts harbours a point-like nuclear X-ray source, which is likely evidence of an accreting nuclear black hole. We use *Chandra* data

Table 1. 33 spiral galaxies with a potential IMBH

| Galaxy | $M_{\text{bh}} (M_{*,\text{total}})$ M_\odot | $M_{\text{bh}} (\phi)$ M_\odot | $M_{\text{bh}} (\sigma)$ M_\odot |
|---|---|-------------------------------------|---------------------------------------|
| 3 estimates $< 10^5 M_\odot$ | | | |
| N4178 | 3×10^4 | 2×10^4 | 1×10^3 |
| N4713 | 9×10^3 | 3×10^3 | 6×10^2 |
| 2 estimates $< 10^5 M_\odot$, no estimate $> 10^5 M_\odot$ | | | |
| IC3392 | 2×10^4 | 6×10^4 | ... |
| N4294 | 2×10^4 | 3×10^3 | ... |
| N4413 | 1×10^4 | 3×10^4 | ... |
| 2 estimates $< 10^5 M_\odot$, 1 estimate $\geq 10^6 M_\odot$ | | | |
| N4424 | 4×10^4 | 5×10^6 | 1×10^5 |
| N4470 | 1×10^4 | 4×10^4 | 1×10^6 |
| 1 estimate $\leq 10^5 M_\odot$, no estimate $> 10^6 M_\odot$ | | | |
| N4197 | 7×10^4 | 2×10^5 | ... |
| N4237 | 5×10^5 | 5×10^4 | 2×10^5 |
| N4298 | 5×10^5 | 4×10^5 | 2×10^4 |
| N4299 | 7×10^3 | 2×10^5 | ... |
| N4312 | 1×10^4 | ... | 3×10^5 |
| N4313 | 2×10^5 | ... | 2×10^5 |
| N4390 | 8×10^3 | 7×10^5 | ... |
| N4411b | 3×10^4 | 4×10^5 | ... |
| N4416 | 9×10^5 | 1×10^4 | ... |
| N4498 | 2×10^4 | 6×10^5 | ... |
| N4519 | 6×10^4 | 3×10^5 | ... |
| N4647 | 4×10^5 | 8×10^5 | 4×10^4 |
| N4689 | 3×10^5 | 3×10^5 | 2×10^4 |
| 1 estimate $\leq 10^5 M_\odot$ | | | |
| IC3322 | 1×10^4 | ... | ... |
| N4206 | 5×10^4 | ... | ... |
| N4222 | 7×10^4 | ... | ... |
| N4330 | 6×10^4 | ... | ... |
| N4356 | $\times 10^5$ | ... | ... |
| N4396 | 2×10^3 | ... | ... |
| N4405 | 6×10^4 | ... | ... |
| N4445 | 2×10^4 | ... | ... |
| N4451 | 1×10^5 | ... | ... |
| N4522 | 2×10^4 | ... | ... |
| N4532 | 1×10^4 | ... | ... |
| N4606 | 3×10^4 | ... | ... |
| N4607 | 3×10^4 | ... | ... |

Uncertainties can reach an order of magnitude, as shown in the Appendix Table A and Figures 6, 8 and 10.

as the primary resource for our search, because *Chandra* is the only X-ray telescope that can provide accurate sub-arcsecond localisations of faint point-like sources (down to $\lesssim 10$ counts), thanks to the low instrumental background of its Advanced CCD Imaging Spectrometer (ACIS). In the absence of *Chandra* data, we inspected archival *XMM-Newton* European Photon Imaging Camera (EPIC) data, particularly in cases when a long EPIC exposure partly made up for the much lower spatial resolution and much higher instrumental and background noise. For the five primary targets identified above, two (NGC 4178 and NGC 4713) have archival *Chandra*/ACIS X-ray data already available, and one (NGC 4294) has *XMM-Newton*/EPIC data. The other two (IC 3392 and NGC 4413) have recently been observed as part of our ongoing *Chandra* survey of the Virgo cluster; the results of the new observations will be presented in a separate paper.

We re-processed and analysed the archival *Chandra* X-ray data using the Chandra Interactive Analysis of Observations (CIAO) Version 4.9 software package (Fruscione et al. 2006). For sources with a sufficient number of counts, we extracted spectra and built

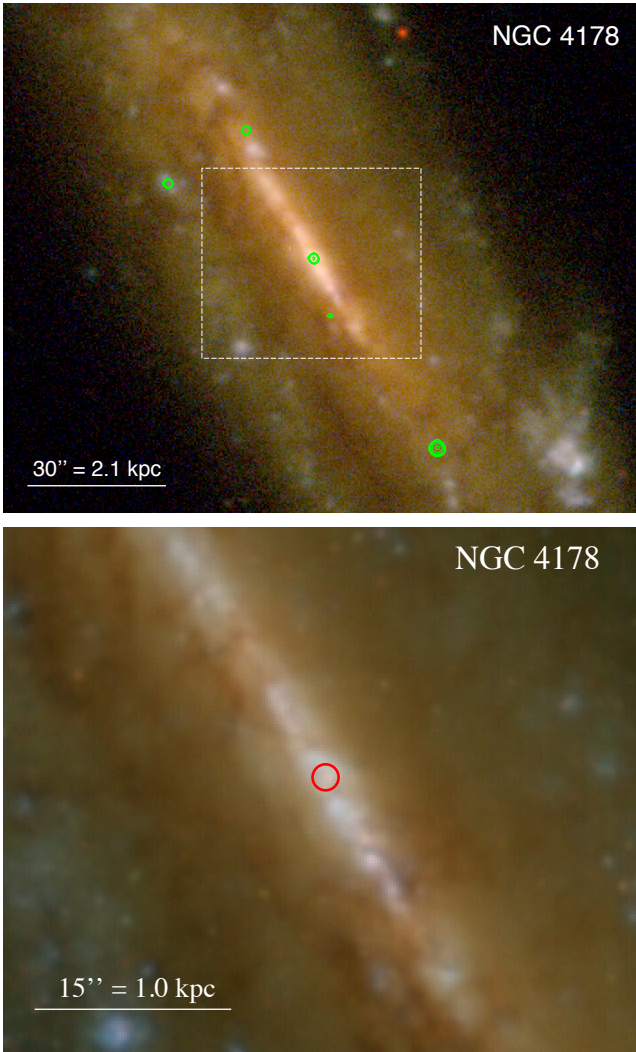


Figure 11. Top panel: SDSS image of NGC 4178 (red = i filter; green = g ; blue = u), with *Chandra*/ACIS-S contours (0.3–7.0 keV band) overlaid in green. North is up, east is to the left. Bottom panel: zoomed-in view of the nuclear region, from the Next Generation Virgo-cluster Survey, with the position of the *Chandra* nuclear source overlaid as a red circle (radius 1'').

response and auxiliary response files with the CIAO task *specextract*, and fitted the spectra with XSPEC version 12.9.1 (Arnaud 1996). For sources with fewer counts, we converted between count rates and fluxes using the Portable, Interactive Multi-Mission Simulator (PIMMS) software Version 4.8e, available online¹⁴ within the *Chandra X-ray Observatory* Proposal Planning Toolkit. X-ray contour plots, aperture photometry, and other imaging analysis was done with the DS9 visualization tool, part of NASA’s High Energy Astrophysics Science Archive Research Center (HEASARC) software. For the archival *XMM-Newton* data, we used standard pipeline products (event files, images, and source lists), downloaded from the HEASARC archive; we also used ds9 for aperture photometry and PIMMS for flux conversions.

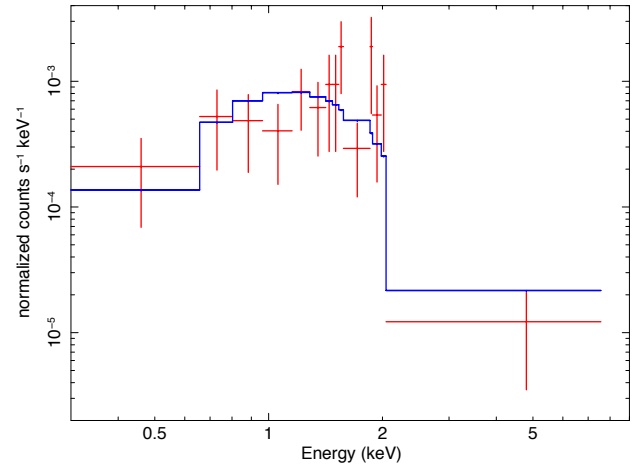


Figure 12. *Chandra*/ACIS-S spectrum of the nuclear source in NGC 4178, fitted with a disk-blackbody model. The datapoints have been grouped to a signal-to-noise >1.5 for plotting purposes only. The fit was done on the individual counts, using Cash statistics. See Section 4.1 for the fit parameters. The sharp drop of detected counts above 2 keV disfavors a power-law model.

5.1 NGC 4178

From the previous sections, we have three predictions for the black hole mass in NGC 4178, and they all point towards a black hole in the mass range 10^3 – $10^4 M_\odot$. This galaxy was observed by *Chandra*/ACIS-S for 36 ks on 2011 February 19 (Cycle 12). We downloaded the data from the public *Chandra* archives, and reprocessed them with the CIAO task *chandra_repro*. We confirm the detection of an X-ray source consistent with both the dynamical centre of the galaxy (Figure 11) and a nuclear star cluster (Satyapal et al. 2009; Secrest et al. 2012, 2013). We extracted the source counts from a circle of radius 2'', and the background counts from an annulus between radii of 3'' and 9''. As discussed by Secrest et al. (2012), this source is unusually soft for an AGN. We measured a net count rate of $(2.8 \pm 0.9) \times 10^{-4}$ ct s $^{-1}$ in the 0.3–1.0 keV band, $(6.2 \pm 1.3) \times 10^{-4}$ ct s $^{-1}$ in the 1.0–2.0 keV band, and $(1.0 \pm 0.6) \times 10^{-4}$ ct s $^{-1}$ in the 2.0–7.0 keV band. With only $\approx 36 \pm 6$ net counts, it is clearly impossible to do any proper spectral fitting, and certainly any fitting based on the χ^2 statistics (which requires $\gtrsim 15$ counts per bin). Nonetheless, we can fit the data with the Cash statistics (Cash 1979), generally used for sources with a small number of counts, and constrain some simple models. Power-law fitting based on the hardness ratio was carried out and discussed in detail by Secrest et al. (2012). We re-fitted the spectrum in XSPEC, with the Cash statistics, after rebinning to 1 count per bin; we confirm that the power-law is steep, i.e. it is a soft spectrum, with photon index $\Gamma = 3.4^{+1.7}_{-1.2}$, with an intrinsic absorbing column density $N_H = 5^{+5}_{-4} \times 10^{21}$ cm $^{-2}$ (C-statistics of 34.2 for 31 degrees of freedom). Such a steep slope, moderately high absorption, and large uncertainty on both parameters make it difficult to constrain the 0.3–10 keV unabsorbed luminosity: formally we obtain a 90% confidence limit of $L_{0.3-10} = 9^{+105}_{-6} \times 10^{38}$ erg s $^{-1}$, consistent with the estimates of Secrest et al. (2012).

However, when we look at the individual detected energy of the few counts, rather than simply considering the hardness ratio, we find that the power-law model is inadequate. The decline in the number of detected counts above 2 keV is very sharp (Figure 12), consistent with the Wien tail of an optically thick thermal spectrum. We therefore fit the same spectrum with an absorbed

¹⁴ <http://cxc.harvard.edu/toolkit/pimms.jsp>

diskbb model: we obtain a C-statistic of 31.5/31 (an improvement at the 90% confidence level, with respect to the power-law fit). The best-fitting parameters are $N_{\text{H}} = 1.5^{+3.3}_{-1.5} \times 10^{21} \text{ cm}^{-2}$ for the intrinsic absorption, $kT_{\text{in}} = 0.56^{+0.35}_{-0.19} \text{ keV}$ for the peak disk temperature, $r_{\text{in}} = 94^{+212}_{-62} (\cos \theta)^{-1/2} \text{ km}$ for the apparent inner-disk radius, where θ is the viewing angle. The unabsorbed luminosity is $L_{0.3-10} = 1.9^{+1.9}_{-0.7} \times 10^{38} \text{ erg s}^{-1}$. Luminosity, temperature, and inner-disk radius are self-consistent for a stellar-mass black hole in the high/soft state. The temperature is too high, and the radius too small, for a supermassive black hole or even an IMBH. Invoking Occam's razor, we argue that the most likely interpretation of the X-ray source at the nuclear location of NGC 4178 is a stellar-mass X-ray binary.

What to make, then, of the strong mid-IR emission in [Ne V] (Satyapal et al. 2009; Secrest et al. 2012), which is usually a signature of strong X-ray photoionisation and was the strongest argument in favour of a hidden AGN in this galaxy? It is always possible to postulate a Compton-thick AGN, powerful enough to supply the required luminosity; we simply argue that this hypothesis is untestable with the available *Chandra* data. Alternatively, the nuclear black hole may have been more active in the recent past (producing the highly-ionised gas around it), but is currently in a low state. The optical line ratios do not require an AGN, either: NGC 4178 is classified as an HII nucleus (Ho et al. 1997; Decarli et al. 2007; Secrest et al. 2012).

The uncertainty on the current luminosity, and indeed on the detection of X-ray emission from the nuclear black hole, makes it impossible to constrain its mass via fundamental-plane relations (Merloni et al. 2003; Plotkin et al. 2012; Miller-Jones et al. 2012). For these relations, Secrest et al. (2013) assumed an intrinsic 0.5–10 keV X-ray luminosity $\approx 10^{40} \text{ erg s}^{-1}$, a bolometric correction factor $\kappa \sim 10^3$, and an upper limit of $84.9 \mu\text{Jy}$ for the 5-GHz flux density; from those values, they predicted a black hole mass $< 8.4 \times 10^4 M_{\odot}$. Instead, we argue that the X-ray luminosity is pure guesswork, with no empirical constraint. Moreover, if the nuclear black hole was indeed an IMBH, the bolometric correction should be much lower than 10^3 ; more likely, $\kappa \lesssim 10$, assuming a peak disk temperature $kT \gtrsim 0.1 \text{ keV}$ for a black hole mass $\lesssim 10^5 M_{\odot}$. In summary, NGC 4178 may host an IMBH but neither the X-ray spectrum of the nuclear source, nor the fundamental plane relations can be used to support this hypothesis.

Alternatively, Secrest et al. (2012) note that the black hole mass may be ~ 0.1 to 1 times the mass of the nuclear star cluster ($M_{\text{nc}} \sim 5 \times 10^5 M_{\odot}$; Satyapal et al. 2009) in this galaxy. This implies $M_{\text{bh}} \sim (0.5 - 5) \times 10^5 M_{\odot}$. We are able to offer an alternative prediction of the black hole mass by using the optimal $M_{\text{bh}}-M_{\text{nc}}$ relation extracted from Graham (2016b), which is such that

$$\log(M_{\text{nc}}/M_{\odot}) = (0.40 \pm 0.13) \times \log(M_{\text{bh}}/[10^{7.89} M_{\odot}]) + (7.64 \pm 0.25). \quad (12)$$

From this, we derive $\log(M_{\text{bh}}/M_{\odot}) = 3.04$ dex. We conclude that this relation offers the best additional support, beyond the initial set of three scaling relations used in the previous section, for an IMBH in NGC 4178. If it has a typical Eddington ratio of say 10^{-6} , then we should not expect to detect it in X-rays (see Paper I).

5.2 NGC 4713

For NGC 4713 (SDSS J124957.86+051841.0), we again have three predictions for the black hole mass, spanning $(0.6-9) \times 10^3 M_{\odot}$.

Based on a 4.9-ks *Chandra*/ACIS-S observation taken on 2003

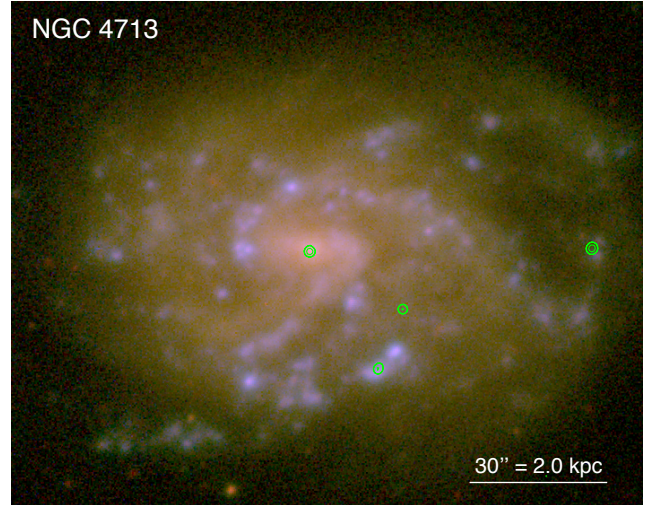


Figure 13. SDSS image of NGC 4713, with *Chandra*/ACIS-S contours overlaid in green. North is up, east is to the left.

January 28 (Cycle 4), Dudik et al. (2005) reported on the lack of a nuclear X-ray source in this dwarf galaxy, with a 0.3–10 keV upper limit of $\approx 4 \times 10^{-4} \text{ ct s}^{-1}$; looking in the mid-IR, Satyapal et al. (2009) also excluded an active nucleus. However, Nagar et al. (2002) had included it in their list of BPT (Baldwin et al. 1981) ‘composite galaxies’, as did Reines, Greene & Geha (2013). Furthermore, Terashima et al. (2015) found an X-ray source at the nuclear position in a 52.2-ks *XMM-Newton* European Photon Imaging Camera observation, part of the *XMM-Newton* Serendipitous Source Catalog Data Release 3 (Watson et al. 2009). The unabsorbed 0.3–10 keV flux is reported as $\approx 5 \times 10^{-14} \text{ erg cm}^{-2} \text{ s}^{-1}$, with the addition of a ‘weak hint’ of an Fe-K line at 6.4 keV. Based on the ratios between the FIR luminosities at $18 \mu\text{m}$ and $90 \mu\text{m}$ (from the AKARI survey; Kawada et al. 2007; Ishihara et al. 2010), and the X-ray luminosity, Terashima et al. (2015) classified the nucleus of NGC 4713 as an unobscured transition object between LINERS and HII nuclei. The lower spatial resolution of *XMM-Newton* makes it impossible to determine whether the faint nuclear X-ray emission is point-like, from an AGN, or extended, from hot gas in a star-forming region.

We reprocessed and re-examined the 4.9-ks *Chandra*/ACIS-S observation. In contrast to the conclusions of Dudik et al. (2005), we do find a point-like X-ray nucleus (see Figure 13), located within $0''.2$ of the optical nucleus as defined by SDSS-DR12 (Alam et al. 2015) and *Gaia* Data Release 2 (Gaia Collaboration et al. 2018). We measure a net count rate in the 0.3–7.0 keV band of $2.0^{+1.3}_{-0.9} \times 10^{-3} \text{ ct s}^{-1}$, i.e. 10 raw counts and 0.2 background counts. The errors reported here are 90% confidence limits calculated from the Tables of Kraft et al. (1991), suitable for sources with a low number of counts. Source counts are detected in all three standard bands (soft, 0.3–1 keV; medium, 1–2 keV; hard, 2–7 keV), which is consistent with a power-law spectrum. Assuming a power-law spectrum with photon index $\Gamma = 1.7$, and line-of-sight column density $N_{\text{H}} = 2 \times 10^{20} \text{ cm}^{-2}$, we find with *rimms* that the net count rate corresponds to a 0.3–10 keV unabsorbed flux of $(1.4^{+0.9}_{-0.6}) \times 10^{-14} \text{ erg cm}^{-2} \text{ s}^{-1}$ (slightly lower than the *XMM-Newton* flux, which may include a hot gas contribution). At the distance of 13.2 Mpc for NGC 4713, this implies a luminosity $L_{0.3-10} = 3.0^{+1.9}_{-1.4} \times 10^{38} \text{ erg s}^{-1}$. We also obtained an essentially identical estimate of $L_{0.5-7} \approx$

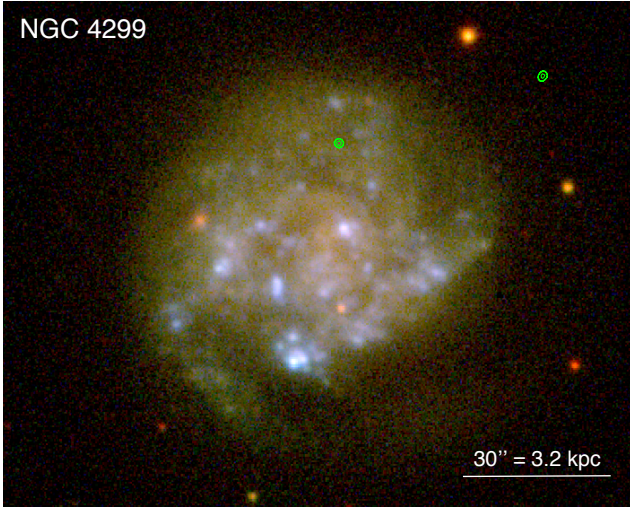


Figure 14. SDSS image of NGC 4299, with *Chandra*/ACIS-S contours overlaid in green (seen to the right of the galaxy). North is up, east is to the left.

$3.1 \times 10^{38} \text{ erg s}^{-1}$ using the *ciao* task *srcflux* within *ds9*, with the same input spectral model and column density.

5.3 Galaxies with 2 BH mass estimates $< 10^5 M_\odot$

NGC 4294 was observed by *XMM-Newton*/EPIC on 2016 June 10, for 46 ks. We found no sources at the nuclear position, in the stacked EPIC pn and MOS image. The nearest point source is located $\approx 9''$ from the optical nuclear position, way beyond the possible astrometric uncertainty of the EPIC image. We estimate a 90% confidence limit for the 0.3–10 keV nuclear luminosity of $L_{0.3-10} < 1 \times 10^{38} \text{ erg s}^{-1}$, for a distance of 17.0 Mpc.

Among the other four galaxies with two black hole mass estimates $< 10^5 M_\odot$ (Table 1), three (IC 3392, NGC 4413, and NGC 4424) have been observed by *Chandra* this year for our Virgo survey, and we will present the results in a separate paper. The fourth galaxy, NGC 4470, was observed by *Chandra* several times between 2010 and 2016: twice with ACIS-I, and four times with ACIS-S. However, in all cases, it was not the primary target of the observation, and was located several arcmin away from the aimpoint, with a resulting degradation of the point spread function at its location. Moreover, in three of the four ACIS-S observations, the nuclear position of NGC 4470 fell onto the less sensitive S2 chip, rather than the S3 chip. Of all the available datasets, the most useful one for our investigation is from a 20-ks observation taken on 2010 November 20 (Cycle 12): it is the only observation in which NGC 4470 is on the S3 chip, only $\approx 4'$ from the aimpoint. From this observation, we found excess emission centred at $\approx 1''$ of the SDSS and *Gaia* optical nuclear positions (smaller than the positional uncertainty of the X-ray source at that off-axis position and for the small observed number of counts), with a net count rate of $(5 \pm 2) \times 10^{-4} \text{ ct s}^{-1}$ (*i.e.*, ≈ 10 net counts) in the 0.3–7.0 keV band. For an absorbing column density $N_H = 1.7 \times 10^{20} \text{ cm}^{-2}$ a power-law photon index $\Gamma = 1.7$, and a distance of 18.8 Mpc, this corresponds to an unabsorbed luminosity $L_{0.3-10} = 2.2^{+1.9}_{-1.2} \times 10^{38} \text{ erg s}^{-1}$.

5.4 Galaxies with 1 BH mass estimate $\lesssim 10^5 M_\odot$

Finally, we examined the 26 galaxies with one black hole mass estimate $\lesssim 10^5 M_\odot$ (Table 1). Twenty of them have been observed

as part of our Virgo survey, and we will report on them elsewhere. The other three, NGC 4299, NGC 4647 and NGC 4689, already had archival *Chandra* data.

NGC 4299 was observed by *Chandra*/ACIS-S on 2007 November 18, for 5.0 ks. We do not find any significant emission at the nuclear position (see Figure 14); we place a 90% upper limit of $8 \times 10^{-4} \text{ count s}^{-1}$ in the 0.3–7 keV band, using the tables of Kraft et al. (1991). Assuming line-of-sight Galactic absorption $N_H = 2.5 \times 10^{20} \text{ cm}^{-2}$, and a power-law spectrum with photon index $\Gamma = 1.7$, this corresponds to a luminosity $L_{0.3-10} < 7 \times 10^{38} \text{ erg s}^{-1}$ at the distance of 21.9 Mpc.

NGC 4647 was observed by *Chandra*/ACIS-S on six visits between 2000 and 2011 (2000 April 20: 38 ks; 2007 January 30: 52 ks; 2007 February 01: 18 ks; 2011 August 08: 85 ks; 2011 August 12: 14 ks; 2011 February 24: 101 ks), for a total of ≈ 308 ks. On all occasions, the aimpoint was located at the main target of the observation, the nearby E galaxy NGC 4649; however, NGC 4647 is only $\approx 2'.5$ away, and falls within the S3 chip in all six datasets. We inspected each observation individually, and we then used the *ciao* script *merge_obs* to create a stacked, exposure-corrected image. We used point-like optical/X-ray associations to align the *Chandra* image onto the SDSS optical image, so that the two frames coincide within $\lesssim 0''.3$. There is no point-like X-ray source at the nuclear location, defined by SDSS (also in agreement with *Gaia*'s nuclear position within the same uncertainty). The nearest point-like X-ray source (most likely an X-ray binary) is located $\approx 3''$ to the west of the nuclear location, well above its positional uncertainty. The 90 percent upper limit of the (undetected) nuclear source is $3.6 \times 10^{-5} \text{ ct s}^{-1}$ in the 0.3–7 keV band. To convert this upper limit into a luminosity limit, we took a weighted average of the contributions over the different observation cycles, to take into account the change in the response of the ACIS detector; we also assumed, as usual, a line-of-sight Galactic absorption (in this case, $N_H = 2.1 \times 10^{20} \text{ cm}^{-2}$) and a power-law spectrum with photon index $\Gamma = 1.7$. We conclude that the nuclear X-ray luminosity is $L_{0.3-10} < 1 \times 10^{37} \text{ erg s}^{-1}$, at the distance of 17.6 Mpc.

NGC 4689 was observed by *Chandra*/ACIS-S for 5 ks on 2007 May 7 (Cycle 8). We do not detect any net emission at the nuclear position; the Bayesian 90% confidence limit on the net count rate is $\approx 5 \times 10^{-4} \text{ ct s}^{-1}$. For a line-of-sight Galactic absorption $N_H = 2.0 \times 10^{20} \text{ cm}^{-2}$ and a photon index $\Gamma = 1.7$, we obtain an upper limit to the nuclear black hole luminosity of $L_{0.3-10} < 1.2 \times 10^{38} \text{ erg s}^{-1}$, at the distance of 16.4 Mpc.

A summary of the X-ray observation exposure times, count rates, and luminosities is provided in Table 2.

6 DISCUSSION

Observational evidence for ~ 12 , 30 and 60 solar mass black holes already exists (Reid et al. 2014; Abbott et al. 2016, 2017). It is also understood that in today's universe, the end product of a massive star will be a 'stellar mass' black hole less than $80\text{--}100 M_\odot$, but near this limit if the star's metallicity was low ($10^{-2}\text{--}10^{-3}$ solar) and the mass loss from its stellar wind was low (Belczynski et al. 2010; Spera et al. 2015; Spera & Mapelli 2017). While some authors have advocated that the seed masses which gave rise to the supermassive black holes at the centres of galaxies started out with masses of $10^5\text{--}10^6 M_\odot$ (e.g. Turner 1991; Loeb & Rasio 1994), and many AGN are known to have $10^5\text{--}10^6 M_\odot$ black holes (e.g. Graham & Scott 2015, and references therein), the assumption that there are not black holes with masses of $10^2\text{--}10^5 M_\odot$ need not hold. The

Table 2. Summary of the X-ray observations used for this work and of their respective nuclear X-ray properties.

| Galaxy | Observatory | Date | Exp Time (ks) | Count Rate ^a (ct s ⁻¹) | $L_{0.3-10}$ (erg s ⁻¹) |
|----------|-------------------|-------------------------|------------------|--|--|
| NGC 4178 | <i>Chandra</i> | 2011-02-19 | 36 | $(1.0^{+0.2}_{-0.2}) \times 10^{-3}$ | $(1.9^{+1.9}_{-0.7}) \times 10^{38}$ |
| NGC 4713 | <i>Chandra</i> | 2003-01-28 | 4.9 | $(2.0^{+1.3}_{-0.9}) \times 10^{-3}$ | $(3.0^{+1.9}_{-1.4}) \times 10^{38}$ |
| NGC 4294 | <i>XMM-Newton</i> | 2006-06-10 | 46 | $< 1 \times 10^{-3}$ | $< 1 \times 10^{38}$ |
| NGC 4470 | <i>Chandra</i> | 2010-11-20 | 20 | $(0.5^{+0.2}_{-0.2}) \times 10^{-3}$ | $(2.2^{+1.9}_{-1.2}) \times 10^{38}$ |
| NGC 4299 | <i>Chandra</i> | 2007-11-18 | 5.0 | $< 0.8 \times 10^{-3}$ | $< 7 \times 10^{38}$ |
| NGC 4647 | <i>Chandra</i> | 2000-04-20 | 38 | | |
| | | 2007-01-30 | 52 | | |
| | | 2007-02-01 | 18 | | |
| | | 2011-02-24 | 101 | | |
| | | 2011-08-08 | 85 | | |
| | | 2011-08-12 (stacked) | 308 | $< 0.036 \times 10^{-3}$ | $< 0.1 \times 10^{38}$ |
| NGC 4689 | <i>Chandra</i> | 2007-05-07 | 5.0 | $< 0.5 \times 10^{-3}$ | $< 1.2 \times 10^{38}$ |

^a For *Chandra* observations: observed ACIS-S count rate in the 0.3–7 keV band; for *XMM-Newton*: observed EPIC-pn count rate in the 0.3–10 keV band.

perceived need for massive seeds was originally invoked because, under the assumption of spherical accretion, there was not sufficient time to grow the massive quasars observed in the early Universe. However, it is possible to grow black holes at a much faster rate than the idealised and restrictive Eddington accretion rate (e.g. Alexander & Natarajan 2014; Nayakshin et al. 2012). Moreover, even if the massive quasars did form from massive seeds (Pacucci et al. 2016), there may still be a continuum of BH masses, perhaps with today’s IMBHs born from Pop III and II.5 stars, or from other processes, as noted in Section 1. There are, therefore, reasons to expect that IMBHs with $10^2 < M_{\text{bh}}/M_{\odot} < 10^5$ should exist.

Just as initial searches for exoplanets found the larger ones first, and surveys of galaxies found the bright Hubble-Jeans sequence (Jeans 1919, 1928; Hubble 1926, 1936) prior to the detection of low surface brightness galaxies, sample selection effects hinder the detection of IMBHs in galactic nuclei. Their gravitational spheres-of-influence are too small to be spatially resolved with our current instrumentation. Furthermore, ambiguity also arises because the energy levels of their current low-accretion activity overlaps with that of highly-accreting stellar mass black holes in X-ray binaries. There is, however, no obvious physical reason why these IMBHs should not exist, and a small number of candidates are known, including the already-mentioned $\sim 10^4 M_{\odot}$ black hole near/inside ESO 243-49 (Farrell et al. 2009; Yan et al. 2015; Webb et al. 2017; Soria et al. 2017), plus the nuclear black holes in LEDA 87300 (Baldassare et al. 2015; whose mass estimate was halved in Graham et al. 2016, see also Baldassare et al. 2017) and in NGC 404 (with a 3σ upper limit on its black hole mass of $1.5 \times 10^5 M_{\odot}$; Nguyen et al. 2017).

There is also a series of studies (Pardo et al. 2016; Mezcua et al. 2016, 2018) which have estimated the masses of distant low mass black holes using a near-linear $M_{\text{bh}}-M_{\text{tot}}$ relation for AGN from Reines & Volonteri (2015). However, it should be noted that Reines & Volonteri (2015) appear unaware of, or reject, the bend in the $M_{\text{bh}}-M_{\text{spheroid}}$ diagram (see Graham & Scott 2015), and the associated bend in the $M_{\text{bh}}-M_{\text{tot}}$ diagram which is evident in the data they present. Fitting a log-linear relation to galaxies that they consider to contain a classical bulge rather than a pseudobulge, the right hand panel of figure 10 in Reines & Volonteri (2015) reveals that all galaxies with $M_{\text{bh}} \lesssim 10^8 M_{\odot}$ (except for the stripped

compact elliptical galaxy M 32 which should be down-weighted in this diagram due to its rare nature relative to normal galaxies) reside below their $M_{\text{bh}}-M_{\text{tot}}$ relation for classical bulges and elliptical galaxies. Many more galaxies with directly measured black hole masses also reside below their relation, but they were labelled “pseudobulges” and excluded by Reines & Volonteri (2015). Given that the bulge-to-total mass ratio tends to decrease as one progresses to lower mass spiral galaxies, the $M_{\text{bh}}-M_{\text{tot}}$ relation for spiral galaxies (Davis et al. 2018b) is steeper than the near-quadratic relation for the bulges of spiral galaxies (e.g. Scott et al. 2013; Savorgan et al. 2016; Davis et al. 2018a). Reines & Volonteri (2015) instead suggest that their AGN sample — used to define their near-linear $M_{\text{bh}}-M_{\text{tot}}$ relation for AGN — reside in pseudobulges that have an $M_{\text{bh}}/M_{\text{tot}}$ ratio of ≈ 0.03 percent at $M_{\text{tot}} = 10^{11} M_{\odot}$. However, their distribution of AGN data does not match the distribution of spiral galaxies (also alleged to contain pseudobulges) with directly measured black hole masses and stellar masses derived from space-based infrared images. As such, while the dwarf galaxies studied by Pardo et al. (2016) and Mezcua et al. (2016, 2018) may contain IMBHs, it may be worthwhile revisiting their black hole masses.

A growing number of alleged and potential IMBHs, not located at the center of their host galaxy, are also known (e.g. Colbert & Mushotzky 1999; Farrell et al. 2009, 2014; Soria et al. 2010; Webb et al. 2010, 2014; Liu et al. 2012; Secrest et al. 2012; Sutton et al. 2012; Kaaret & Feng 2013; Miller et al. 2013; Cseh et al. 2015; Mezcua et al. 2015; Oka et al. 2016; Pasham et al. 2014, 2015). It has been theorised that some of these may have previously resided at the centre of a galaxy: perhaps from a stripped satellite galaxy or minor merger (e.g. Drinkwater et al. 2003), or perhaps they were dynamically ejected from the core of their host galaxy (e.g. Merritt et al. 2009). This latter phenomenon may occur due to the gravitational recoiling of a merged black hole pair (e.g. Bekenstein 1973; Favata et al. 2004; Herrmann et al. 2007; Nagar 2013). Alternatively, or additionally, IMBHs may have formed in their off-centre location. Such speculation should, however, be tempered at this point because, as noted in Section 1, many such past IMBH candidates can be explained as super-Eddington accretion onto stellar-mass compact objects (Feng & Soria 2011; Kaaret et al. 2017).

There are many methods, beyond those already employed here, that can be used to identify, and probe the masses of, black holes. This includes reverberation mappings of AGN (e.g. Bahcall, Kozlovsky & Salpeter 1972; Blandford & McKee 1982; Netzer & Peterson 1997), the ‘fundamental plane of black hole activity’ (Merloni et al. 2003; Falcke et al. 2004), spectral modelling of the high-energy X-ray photon coming from the hot accretion discs around IMBHs (Pringle & Rees 1972; Narayan & Yi 1995), high-ionization optical emission lines (Baldwin et al. 1981; Kewley et al. 2001); and high spatial resolution observations of maser emission using radio and millimetre/submillimetre interferometry (e.g. Miyoshi et al. 1995; Greenhill et al. 2003; Humphreys et al. 2016; Asada et al. 2017). In addition, the merging of black holes is now quite famously known to produce gravitational radiation during their orbital decay (Abbott et al. 2016). The merging of galaxies containing their own central IMBH is similarly expected to result in the eventual merging of these black holes. The Kamioka Gravitational Wave Detector (KAGRA: Aso et al. 2013) will be a 3-km long underground interferometer in Japan that is capable of detecting the gravitational radiation emanating from collisions involving black holes with masses up to $200 M_{\odot}$ (Tápai et al. 2015). The planned Deci-Hertz Interferometer Gravitational wave Observatory (DECIGO: Kawamura et al. 2011) and the European, Laser Interferometer Space Antenna (LISA) Pathfinder mission¹⁵ (Anza et al. 2005; McNamara 2013), with their greater separation of mirrors, will be able to detect longer wavelength gravitational waves, and thus better reach into the domain of intermediate-mass and super-massive black hole mergers, the latter of which are currently being searched for via ‘pulsar timing arrays’ (PTAs) (e.g. Hobbs et al. 2010; Kramer & Champion 2013; Shannon et al. 2015). A key constraint to the expected detection threshold of such signals from PTAs – in particular the background of cosmic ripples from the merger of massive black holes (themselves arising from the merger of galaxies) – is the (black hole)-to-(host galaxy/bulge) mass ratio (see equation (4) for spiral galaxies). An additional source of long wavelength gravitational radiation will arise from the inspiral of compact stellar mass objects, such as neutron stars and black holes, around these IMBHs (Mapelli et al. 2012). It is reasonable to expect that the densely packed nuclear star clusters, which coexist with low-mass SMBHs (e.g. González Delgado et al. 2008; Seth et al. 2008; Graham & Spitler 2009), will similarly surround many IMBHs. Gravitational radiation, and the gravitational tidal disruption of ill-fated stars that venture too close to these black holes (Komossa et al. 2009, Komossa 2013 and references therein; Zhong et al. 2015; Stone & Metzger 2016; Lin et al. 2018), are therefore expected from these astrophysical entities. There is, therefore, an array of future observations which could yield further confidence and insight into the realm of IMBHs.

In the pursuit of galaxies that may harbour (some of) the largely missing population of IMBHs, we have predicted the black hole masses in 74 spiral galaxies in the Virgo cluster that will be imaged with the ACIS-S detector on the *Chandra X-ray Observatory*. Previously, Gallo et al. (2008) performed a complementary investigation looking at 100 early-type galaxies in the Virgo cluster. However, they only used two global properties of the galaxies (σ and $M_{*,\text{galaxy}}$) to predict the black hole masses, and their predictions differed systematically and significantly from each other (Gallo et al. 2008, their figure 4), revealing that either one, or both, of their black hole scaling relations was in error. That offset, which reached

Table 3. Black hole calibration points

| M_{bh} M_{\odot} | $M_{*,\text{total}}$ M_{\odot} | ϕ [deg] | σ km s^{-1} |
|--------------------------------|---|-----------------|--------------------------------|
| 10^9 | 2.9×10^{11} (2.4×10^{11}) | 3.0 | 293 |
| 10^8 | 1.2×10^{11} (1.1×10^{11}) | 9.1 | 195 |
| 10^7 | 5.1×10^{10} (5.3×10^{10}) | 15.2 | 130 |
| 10^6 | 2.1×10^{10} (2.5×10^{10}) | 21.3 | 86 |
| 10^5 | 8.9×10^9 (1.2×10^{10}) | 27.4 | 57 |
| 10^4 | 3.7×10^9 (5.5×10^9) | 33.5 | 38 |
| 10^3 | 1.6×10^9 (2.6×10^9) | 39.6 | 25 |
| 10^2 | 6.6×10^8 (1.2×10^8) | 45.7 | 17 |

Reversing equations 4 (5), 2 and 3, we provide the total galaxy stellar mass, spiral arm pitch angle and stellar velocity dispersion that corresponds to the black hole masses listed in column 1, respectively.

3 orders of magnitude at the low mass end, is investigated and reconciled in Paper I. Here, we have used three global properties of spiral galaxies (σ , $M_{*,\text{galaxy}}$ and spiral arm pitch angle ϕ) to predict the black hole masses in our spiral galaxy sample. Moreover, our updated scaling relations are internally consistent with each other and do not contain any dramatic systematic bias. Table 3 provides a sense of what galaxy parameter values are associated with a given set of black hole masses. Based on our estimates of these galaxies’ stellar masses, 33 of the 74 galaxies are predicted to have a black hole mass less than 10^5 – $10^6 M_{\odot}$ (see Table 1).

The black hole mass estimates presented here shall be used in a number of forthcoming papers once imaging from the new *Chandra* Cycle 18 Large Project ‘Spiral galaxies of the Virgo cluster’ (Proposal ID: 18620568) is completed. Given the low degree of scatter about the $M_{\text{bh}}-\phi$ relation, it appears to be the most promising relation to use in the search for IMBHs in late-type galaxies. In future work, we intend to identify those late-type spiral galaxies with open, loosely-wound spiral arms, i.e. those expected to have the lowest mass black holes at their centre, and then check for the signature of a hot accretion disk heralding the presence of potentially further IMBHs.

ACKNOWLEDGEMENTS

This research was supported under the Australian Research Council’s funding scheme DP17012923. Part of this research was conducted within the Australian Research Council’s Centre of Excellence for Gravitational Wave Discovery (OzGrav), through project number CE170100004. Support for this work was provided by the National Aeronautics and Space Administration through Chandra Award Number 18620568. This research has made use of the NASA/IPAC Extragalactic Database (NED). This publication makes use of data products from the Two Micron All Sky Survey. We acknowledge use of the HyperLeda database (<http://leda.univ-lyon1.fr>). This research has made use of the GOLDMine Database.

REFERENCES

- Abbott, B. P., Abbott, R., Abbott, T. D., et al. 2016, *Physical Review Letters*, 116, 061102
- Abbott, B. P., Abbott, R., Abbott, T. D., et al. 2017, *Physical Review Letters*, 118, 221101
- Alam, S., Albareti, F. D., Allende Prieto, C., et al. 2015, *ApJS*, 219, 12
- Alexander, T., & Natarajan, P. 2014, *Science*, 345, 1330
- Alvarez, M. A., Wise, J. H., & Abel, T. 2009, *ApJ*, 701, L133

¹⁵ <http://sci.esa.int/lisa-pathfinder/>

- Anderson J., van der Marel R.P. 2010, *ApJ*, 710, 1032
- Anza, S., Armano, M., Balaguer, E., et al. 2005, *Classical and Quantum Gravity*, 22, 125
- Argyres, P. C., Dimopoulos, S., & March-Russell, J. 1998, *Physics Letters B*, 441, 96
- Arnaud K.A., 1996, *ASPC*, 101, 17
- Asada, K., Kino, M., Honma, M., et al. 2017, *arXiv:1705.04776*
- Aso, Y., Michimura, Y., Somiya, K., et al. 2013, *Physical Review D*, 88, 043007
- Bahcall J.N., Kozlovsky B.Z., Salpeter E.E., 1972, *ApJ*, 171, 467
- Baldassare, V. F., Reines, A. E., Gallo, E., & Greene, J. E. 2015, *ApJ*, 809, L14
- Baldwin, J. A., Phillips, M. M., & Terlevich, R. 1981, *PASP*, 93, 5
- Bean, R., & Magueijo, J. 2002, *Phys. Rev. D*, 66, 063505
- Bekenstein, J. D. 1973, *ApJ*, 183, 657
- Belczynski, K., Bulik, T., Fryer, C. L., et al. 2010, *ApJ*, 714, 1217
- Bell, E. F., McIntosh, D. H., Katz, N., & Weinberg, M. D. 2003, *ApJS*, 149, 289
- Bell, E. F., & de Jong, R. S. 2001, *ApJ*, 550, 212
- Berrier, J. C., Davis, B. L., Kennefick, D., et al. 2013, *ApJ*, 769, 132
- Blandford R.D., McKee C.F., 1982, *ApJ*, 255, 419
- Bond, J. R., Arnett, W. D., & Carr, B. J. 1984, *ApJ*, 280, 825
- Bromm, V., & Loeb, A. 2003, *The Emergence of Cosmic Structure*, 666, 73
- Carr, B. J., Bond, J. R., & Arnett, W. D. 1984, *ApJ*, 277, 445
- Carr, B. J., Kohri, K., Sendouda, Y., & Yokoyama, J. 2010, *Phys. Rev. D*, 81, 104019
- Cash W. 1979, *ApJ*, 228, 939
- Chabrier, G. 2003, *PASP*, 115, 763
- Clark, G. W., Markert, T. H., & Li, F. K. 1975, *ApJ*, 199, L93
- Colbert, E. J. M., & Mushotzky, R. F. 1999, *ApJ*, 519, 89
- Conroy, C., Gunn, J. E., & White, M. 2009, *ApJ*, 699, 486
- Cseh, D., Webb, N. A., Godet, O., et al. 2015, *MNRAS*, 446, 3268
- Davies, R.L., Efstathiou, G., Fall, S.M., et al. 1983, *ApJ*, 266, 41
- Davis, B. L., Berrier, J. C., Shields, D. W., et al. 2012, *ApJS*, 199, 33
- Davis, B. L., Graham, A. W., & Cameron, E. 2018a, *ApJ*, submitted, *arXiv:1810.04887*
- Davis, B. L., Graham, A. W., & Cameron, E. 2018b, *ApJ*, submitted, *arXiv:1810.04888*
- Davis, B. L., Graham, A. W., & Seigar, M. S. 2017, *MNRAS*, 471, 2187
- Davis S.W., Narayan R., Zhu Y., Barret D., Farrell S.A., Godet O., Servillat M., Webb N.A. 2011, *ApJ*, 734, 111
- Decarli R., Gavazzi G., Arosio I., Cortese L., Boselli A., Bonfanti C., Colpi M. 2007, *MNRAS*, 381, 136
- den Brok, M., Seth, A. C., Barth, A. J., et al. 2015, *ApJ*, 809, 101
- de Vaucouleurs, G., de Vaucouleurs, A., Corwin, H. G. Jr, Buta R. J., Paturel G., & Fouque P. 1991, *Third Reference Catalogue of Bright Galaxies*. Springer-Verlag, Berlin (RC3)
- Doroshkevich, A. G., Zel'dovich, Ya. B., and Novikov, I. D. 1967, *Astr. Zh.*, 44, 295 (Transl., in *Soviet Astr.*, 11, 233, 1967).
- Drinkwater, M. J., Gregg, M. D., Hlker, M., et al., 2003, *Nature*, 423, 519
- Driver, S. P., Popescu, C. C., Tuffs, R. J., et al. 2007, *MNRAS*, 379, 1022
- Driver, S. P., Popescu, C. C., Tuffs, R. J., et al. 2008, *ApJ*, 678, L101
- Dudik R.P., Satyapal S., Gliozzi M., Sambruna R.M. 2005, *ApJ*, 620, 113
- Falcke, H., K rding, E., & Markoff, S. 2004, *A&A*, 414, 895
- Farrell, S.A., Webb, N.A., Barret, D., Godet, O., & Rodrigues, J.M. 2009, *Nature*, 460, 73
- Farrell S.A., Servillat M., Gladstone J.C., et al. 2014, *MNRAS*, 437, 1208
- Favata, M., Hughes, S. A., & Holz, D. E. 2004, *ApJ*, 607, L5
- Feng H., Soria R. 2011, *NewAR*, 55, 166
- Ferrarese, L., & Ford, H. 2005, *Space Sci. Rev.*, 116, 523
- Filippenko, A. V., & Ho, L. C. 2003, *ApJ*, 588, L13
- Fraser, M., Casey, A. R., Gilmore, G., Heger, A., & Chan, C. 2017, *MNRAS*, 468, 418
- Fruscione A., et al. 2006, *SPIE*, 6270, 1
- Gaia Collaboration, Brown, A. G. A., Vallenari, A., et al. 2018, *A&A*, 616, A1
- Gallo, E., Treu, T., Jacob, J., et al. 2008, *ApJ*, 680, 154-168
- Gallo, E., Treu, T., Marshall, P. J., et al. 2010, *ApJ*, 714, 25
- Gavazzi, G., Boselli, A., Donati, A., Franzetti, P., & Scodeggio, M. 2003, *A&A*, 400, 451
- Godet O., et al. 2012, *ApJ*, 752, 34
- Gonz lez Delgado, R. M., P rez, E., Cid Fernandes, R., & Schmitt, H. 2008, *AJ*, 135, 747
- Graham, A. W. 2016a, in *Galactic Bulges*, E. Laurikainen, R.F. Peletier, and D.A. Gadotti (eds.), Springer Publishing, Astrophysics and Space Science Library, v.418, p.263-313
- Graham, A. W. 2016b, *Star Clusters and Black Holes in Galaxies across Cosmic Time*, 312, 269
- Graham, A. W., Ciambur, B. C., & Soria, R. 2016, *ApJ*, 818, 172
- Graham, A. W., & Driver, S. P. 2007, *ApJ*, 655, 77
- Graham, A. W., Jerjen, H., & Guzm n, R. 2003, *AJ*, 126, 1787
- Graham, A. W., Janz, J., Penny, S. J., et al. 2017, *ApJ*, 840, 68
- Graham, A. W., & Scott, N. 2013, *ApJ*, 764, 151
- Graham, A. W., & Scott, N. 2015, *ApJ*, 798, 54
- Graham, A. W., & Soria, R. 2018, *MNRAS*, submitted (Paper I)
- Graham, A. W., & Spitler, L. R. 2009, *MNRAS*, 397, 2148
- Greenhill, L. J., Booth, R. S., Ellingsen, S. P., et al. 2003, *ApJ*, 590, 162
- Grobov, A. V., Rubin, S. G., Samarchenko, D. A., & Zhizhin, E. D. 2011, *Gravitation and Cosmology*, 17, 181
- G rkan M.A., Freitag M., Rasio F.A., 2004, *ApJ*, 604, 632
- Haehnelt, M. G., & Rees, M. J. 1993, *MNRAS*, 263, 168
- Heckman, T. M., & Best, P. N. 2014, *ARA&A*, 52, 589
- Herrmann, F., Hinder, I., Shoemaker, D., Laguna, P., & Matzner, R. A. 2007, *ApJ*, 661, 430
- Ho L.C., Filippenko A.V., Sargent W.L. 1997, *ApJS*, 112, 315
- Hobbs, G., Archibald, A., Arzoumanian, Z., et al. 2010, *Classical and Quantum Gravity*, 27, 084013
- Hubble, E. 1926, *ApJ*, 64, 321
- Hubble, E.P. 1936a, *Realm of the Nebulae*, by E.P. Hubble, New Haven: Yale University Press
- Humphreys, E. M. L., Vlemmings, W. H. T., Impellizzeri, C. M. V., et al. 2016, *A&A*, 592, L13
- Ishihara, D., Onaka, T., Katata, H., et al. 2010, *A&A*, 514, A1
- Iwasawa, K., Fabian, A. C., Almaini, O., et al. 2000, *MNRAS*, 318, 879
- Iye, M., Okamura, S., Hamabe, M., & Watanabe, M. 1982, *ApJ*, 256, 103
- Jarrett, T.H., Chester, T., Cutri, R., et al. 2000, *AJ*, 119, 2498 (2MASS)
- Jeans J. 1919. *Problems of Cosmogony and Stellar Dynamics*, Cambridge: Cambridge Univ. Press
- Jeans, J.H. 1928, *Astronomy & Cosmogony*, (Cambridge: Cambridge University Press), p.332
- Jiang, N., Wang, T., Zhou, H., et al. 2018, *ApJ*, in press
- Johnson, J. L., & Bromm, V. 2007, *MNRAS*, 374, 1557
- Kaaret, P., & Feng, H. 2013, *ApJ*, 770, 20
- Kaaret P., Feng, H., Roberts, T.P., 2017, *ARA&A*, 55, 303
- Kalnajs, A. J. 1975, *La Dynamique des galaxies spirales*, 241, 103
- Kawada, M., Baba, H., Barthel, P. D., et al. 2007, *PASJ*, 59, S389
- Kawamura, S., Ando, M., Seto, N., et al. 2011, *Classical and Quantum Gravity*, 28, 094011
- Kennicutt, R. C., Jr. 1981, *AJ*, 86, 1847
- Kewley, L. J., Dopita, M. A., Sutherland, R. S., Heisler, C. A., & Trevena, J. 2001, *ApJ*, 556, 121
- Kirby, E. M., Jerjen, H., Ryder, S. D., & Driver, S. P. 2008, *AJ*, 136, 1866
- Kiziltan B., Baumgardt H., Loeb A. 2017, *Natur*, 542, 203
- Koliopanos, F., Ciambur, B. C., Graham, A. W., et al. 2017, *A&A*, 601, A20
- Komossa, S. 2013, *IAU Symposium*, 290, 53
- Komossa, S., Zhou, H., Rau, A., et al. 2009, *ApJ*, 701, 105
- Kormendy, J., & Ho, L. C. 2013, *ARA&A*, 51, 511
- Koushiappas, S. M., Bullock, J. S., & Dekel, A. 2004, *MNRAS*, 354, 292
- Kraft R.P., Burrows D.N., Nousek J.A. 1991, *ApJ*, 374, 344
- Krakow, W., Huntley, J. M., & Seiden, P. E. 1982, *AJ*, 87, 203
- Kramer, M., & Champion, D. J. 2013, *Classical and Quantum Gravity*, 30, 224009
- Laine, S., Knapen, J. H., Mu oz-Mateos, J.-C., et al. 2014, *MNRAS*, 444, 3015
- Larson, R. B. 1970, *MNRAS*, 150, 93
- Larson, R. B. 1998, *MNRAS*, 301, 569

- Lin, D., Strader, J., Carrasco, E. R., et al. 2018, *Nature Astronomy*, 2, 656
- Liu, J., Orosz, J., & Bregman, J. N. 2012, *ApJ*, 745, 89
- Loeb, A., & Rasio, F. A. 1994, *ApJ*, 432, 52
- Madau, P., & Rees, M. J. 2001, *ApJ*, 551, L27
- Mapelli, M., Ripamonti, E., Vecchio, A., Graham, A. W., & Gualandris, A. 2012, *A&A*, 542, A102
- Mapelli M., Annibali F., Zampieri L., Soria R. 2013, *A&A*, 559, 124
- Matković, A., & Guzmán, R. 2005, *MNRAS*, 362, 289
- Mayer, L., Kazantzidis, S., Escala, A., & Callegari, S. 2010, *Nature*, 466, 1082
- McNamara, P. W. 2013, *International Journal of Modern Physics D*, 22, 41001
- Meidt, S. E., Schinnerer, E., van de Ven, G., et al. 2014, *ApJ*, 788, 144
- Merloni A., Heinz S., di Matteo T. 2003, *MNRAS*, 345, 1057
- Merritt, D., Schnittman, J. D., & Komossa, S. 2009, *ApJ*, 699, 1690
- Mezcua, M. 2017, *International Journal of Modern Physics D*, 26, 1730021
- Mezcua, M., Roberts, T. P., Lobanov, A. P., & Sutton, A. D. 2015, *MNRAS*, 448, 1893
- Mezcua, M., Civano, F., Fabbiano, G., Miyaji, T., & Marchesi, S. 2016, *ApJ*, 817, 20
- Mezcua, M., Civano, F., Marchesi, S., et al. 2018, *MNRAS*, 478, 2576
- Miller, M. C., & Colbert, E. J. M. 2004, *International Journal of Modern Physics D*, 13, 1
- Miller J.M., Fabbiano G., Miller M.C., Fabian A.C. 2003, *ApJ*, 585, L37
- Miller, J. M., Walton, D. J., King, A. L., et al., 2013, *ApJL*, 776, L36
- Miller-Jones J.C.A., et al. 2012, *ApJ*, 755, L1
- Miyoshi, M., Moran, J., Herrnstein, J., et al. 1995, *Nature*, 373, 127
- Nagar, N. M., Falcke, H., Wilson, A. S., & Ulvestad, J. S. 2002, *A&A*, 392, 53
- Nagar, A. 2013, *Phys. Rev. D*, 88, 121501
- Narayan, R., & Yi, I. 1995, *ApJ*, 452, 710
- Nayakshin, S., Power, C., & King, A. R. 2012, *ApJ*, 753, 15
- Netzer H., Peterson B.M., 1997, in *Astronomical Time Series*, ed. D. Maoz, A. Sternberg, & E.M. Leibowitz (Dordrecht: Kluwer), 85
- Nguyen, D. D., Seth, A. C., den Brok, M., et al. 2017, *ApJ*, 836, 237
- Nucita, A. A., Manni, L., De Paolis, F., Giordano, M., & Ingrassio, G. 2017, *ApJ*, 837, 66
- Oka, T., Mizuno, R., Miura, K., Takekawa, S. 2016, *ApJ*, 816, L7
- Pacucci, F., Ferrara, A., Grazian, A., et al. 2016, *MNRAS*, 459, 1432
- Pardo, K., Goulding, A. D., Greene, J. E., et al. 2016, *ApJ*, 831, 203
- Pasham, D. R., Strohmayer, T. E., & Mushotzky, R. F. 2014, *Nature*, 513, 74
- Pasham, D.R., Cenko, S.B., Zoghbi, A., Mushotzky, R.F., Miller, J., Tombesi, F. 2015, *ApJL*, 811, L11
- Pastorini, G., Marconi, A., Capetti, A., et al. 2007, *A&A*, 469, 405
- Paturel G., Petit C., Prugniel P., Theureau G., Rousseau J., Brouty M., Dubois P., & Cambrésy L. 2003, *A&A* 412, 45
- Plotkin R.M., Markoff S., Kelly B.C., Kording E., Anderson S.F. 2012, *MNRAS*, 419, 267
- Portegies Zwart S.F., McMillan S.L.W. 2002, *ApJ*, 576, 899
- Pour-Imani, H., Kennefick, D., Kennefick, J., et al. 2016, *ApJ*, 827, L2
- Pringle, J. E., & Rees, M. J. 1972, *A&A*, 21, 1
- Press, W. H., Teukolsky, S. A., Vetterling, W. T., & Flannery, B. P. 1992, *Cambridge: University Press*, 1992, 2nd ed.,
- Puerari, I., & Dottori, H. A. 1992, *A&AS*, 93, 469
- Querejeta, M., Meidt, S. E., Schinnerer, E., et al. 2015, *ApJS*, 219, 5
- Quinlan, G. D., & Shapiro, S. L. 1990, *ApJ*, 356, 483
- Rees, M. J. 1984, *ARA&A*, 22, 471
- Regan, J. A., Visbal, E., Wise, J. H., et al. 2017, *Nature Astronomy*, 1, 0075
- Reid, M. J., McClintock, J. E., Steiner, J. F., et al. 2014, *ApJ*, 796, 2
- Reines, A. E., Greene, J. E., & Geha, M. 2013, *ApJ*, 775, 116
- Reines, A. E., & Volonteri, M. 2015, *ApJ*, 813, 82
- Ringermacher, H. I., & Mead, L. R. 2009, *AJ*, 137, 4716
- Roediger, J. C., & Courteau, S. 2015, *MNRAS*, 452, 3209
- Saglia, R. P., Opitsch, M., Erwin, P., et al. 2016, *ApJ*, 818, 47
- Satyapal S., Böker T., Mcalpine W., Gliozzi M., Abel N.P., Heckman T. 2009, *ApJ*, 704, 439
- Savorgnan, G. A. D. 2016, *ApJ*, 821, 88
- Savorgnan, G. A. D., & Graham, A. W. 2015, *MNRAS*, 446, 2330
- Savorgnan, G. A. D., & Graham, A. W. 2016, *ApJS*, 222, 10
- Savorgnan, G. A. D., Graham, A. W., Marconi, A., & Sani, E. 2016, *ApJ*, 817, 21
- Schlaflly, E. F., & Finkbeiner, D. P. 2011, *ApJ*, 737, 103
- Schneider, R., Ferrara, A., Natarajan, P., & Omukai, K. 2002, *ApJ*, 571, 30
- Schombert, J. 2011, arXiv:1107.1728
- Schombert, J. M., Pildis, R. A., Eder, J. A., & Oemler, A., Jr. 1995, *AJ*, 110, 2067
- Schwarzschild, M., & Spitzer, L. 1953, *The Observatory*, 73, 77
- Scott, N., Graham, A. W., & Schombert, J. 2013, *ApJ*, 768, 76
- Secrest N.J., Satyapal S., Gliozzi M., Cheung C.C., Seth A.C., Böker T. 2012, *ApJ*, 753, 38
- Secrest N.J., Satyapal S., Moran S.M., Cheung C.C., Giroletti M., Gliozzi M., Bergmann M.P., Seth A.C. 2013, *ApJ*, 777, 139
- Seigar, M. S., Block, D. L., Puerari, I., Chorney, N. E., & James, P. A. 2005, *MNRAS*,
- Seigar, M. S., Kennefick, D., Kennefick, J., & Lacy, C. H. S. 2008, *ApJ*, 678, L93
- Seth, A., Agüeros, M., Lee, D., & Basu-Zych, A. 2008, *ApJ*, 678, 116-130
- Shankar, F., Salucci, P., Granato, G. L., De Zotti, G., & Danese, L. 2004, *MNRAS*, 354, 1020
- Shannon, R. M., Ravi, V., Lentati, L. T., et al. 2015, *Science*, 349, 1522
- Shapiro, S. L., & Teukolsky, S. A. 1985, *ApJ*, 292, L41
- Shih, D. C., Iwasawa, K., & Fabian, A. C. 2003, *MNRAS*, 341, 973
- Sijacki, D., Springel, V., Di Matteo, T., & Hernquist, L. 2007, *MNRAS*, 380, 877
- Soria, R., Hau, G.K.T., Graham, A.W., Kong, A.K.H., Kuin, N.P.M., Li, I.-H., Liu, J.-F. & Wu, K. 2010, *MNRAS*, 405, 870
- Soria R., Musaeva A., Wu K., Zampieri L., Federle S., Urquhart R., van der Helm E., Farrell S.A. 2017, *MNRAS*, 469, 886
- Spera M., Mapelli M., Bressan A., 2015, *MNRAS*, 451, 4086
- Spera M., Mapelli M., 2017, *MNRAS*, 470, 4739
- Stone, N. C., & Metzger, B. D. 2016, *MNRAS*, 455, 859
- Strader J., Chomiuk L., Maccarone T.J., Miller-Jones J.C.A., Seth A.C., Heinke C.O., Sivakoff G.R. 2012, *ApJ*, 750, L27
- Sutton, A. D., Roberts, T. P., Walton, D. J., Gladstone, J. C., & Scott, A. E. 2012, *MNRAS*, 423, 1154
- Swartz D.A., Soria R., Tennant A.F., 2008, *ApJ*, 684, 282
- Tadhunter, C., Marconi, A., Axon, D., et al. 2003, *MNRAS*, 342, 861
- Tápai, M. K., Zoltán Gergely, László Á. 2015, *Thirteenth Marcel Grossmann Meeting*, eds. Rosquist Kjell et al., Published by World Scientific Publishing, 957 (arXiv:1212.4973)
- Taylor, E. N., Hopkins, A. M., Baldry, I. K., et al. 2011, *MNRAS*, 418, 1587
- Terashima Y., Hirata Y., Awaki H., Oyabu S., Gandhi P., Toba Y., Matsuhara H. 2015, *ApJ*, 814, 11
- Tremaine, S., Gebhardt, K., Bender, R., et al. 2002, *ApJ*, 574, 740
- Turner, E. L. 1991, *AJ*, 101, 5
- Umeda, H., & Nomoto, K. 2003, *Nature*, 422, 871
- Umehara, M., Loeb, A., & Turner, E. L. 1993, *ApJ*, 419, 459
- Watson M.G., et al. 2009, *A&A*, 493, 339
- Webb N.A., Barret D., Godet O., Servillat M., Farrell S.A., Oates S.R. 2010, *ApJ*, 712, L107
- Webb N.A., Godet O., Wiersema K., Lasota J.-P., Barret D., Farrell S.A., Maccarone T.J., Servillat M. 2014, *ApJ*, 780, 9
- Webb N.A., et al. 2017, *A&A*, 602, A103
- Willmer, C.N.A. 2018, *ApJS*, submitted (arXiv:1804.07788)
- Yan, Z., Zhang, W., Soria, R., Altamirano, D., & Yu, W. 2015, *ApJ*, 811, 23
- Yu, S.-Y., Ho, L. C., Barth, A. J., & Li, Z.-Y. 2018, arXiv:1806.06591
- ZelâĖzdovich, Ya. B., and Podurets, M. A. 1965, *Astr. Zh.*, 42, 963 (English translation in *Soviet Astr. J.*, 9, 742) (ZP).
- Zhong, S., Berczik, P., & Spurzem, R. 2015, *ApJ*, 811, 22
- Zolotukhin, I., Webb, N. A., Godet, O., Bachetti, M., & Barret, D. 2016, *ApJ*, 817, 88

**APPENDIX A: GALAXY SAMPLE AND PREDICTED
BLACK HOLE MASSES**

This paper has been typeset from a \LaTeX file prepared by the author.

Table A1. Predicted black hole masses

| Galaxy | Type | Dist.Mod. | $ \phi $ (band) [deg] | $\log M_{\text{bh}}(\phi)$ [dex] | σ km s ⁻¹ | $\log M_{\text{bh}}(\sigma)$ [dex] | $\log M_{*,\text{gal}}$ [dex] | $\log M_{\text{bh}}(M_{*,\text{gal}})$ [dex] |
|--------------------|-----------|-----------|---------------------------------------|---------------------------------------|--------------------------------|---------------------------------------|----------------------------------|---|
| IC3322 | SAB(s)cd | 31.7±0.2 | ... | ... | ... | ... | 9.6±0.1 | 4.0±0.7 (3.5±0.8) |
| IC3322A | SB(s)cd | 31.9±0.4 | ... | ... | ... | ... | 10.1±0.2 | 5.4±0.8 (5.1±0.9) |
| IC3392 | SAB | 30.7±0.5 | 28.2± 3.9 (GALEX/FUV) | 4.8±0.8 | ... | ... | 9.7±0.2 | 4.3±0.9 (3.8±1.0) |
| N4178 | SB(rs)dm | 30.7±0.4 | 31.6± 9.3 (Spitzer/IRAC3) | 4.2±1.6 | 26.0± 3.9 | 3.1±0.9 | 9.7±0.2 | 4.4±0.8 (4.0±0.9) |
| N4192 | SAB(s)ab | 30.7±0.4 | ... | ... | 129.0±19.4 | 7.0±0.7 | 10.7±0.2 | 7.0±1.0 (7.0±1.0) |
| N4197 | Sd | 32.2±0.3 | 24.6± 5.0 (SDSS/g) | 5.4±0.9 | ... | ... | 9.9±0.1 | 4.8±0.8 (4.4±0.8) |
| N4206 | SA(s)bc | 31.3±0.4 | ... | ... | ... | ... | 9.8±0.2 | 4.7±0.8 (4.2±0.9) |
| N4212 | SAc | 31.3±0.3 | 21.5± 1.1 (Spitzer/IRAC2) | 5.9±0.4 | 61.0± 9.2 | 5.1±0.8 | 10.4±0.1 | 6.2±0.8 (6.1±0.9) |
| N4216 | SAB(s)b | 31.0±0.3 | 20.5±10.8 (Spitzer/IRAC2) | 6.1±1.9 | 196.0±29.4 | 8.0±0.6 | 10.9±0.1 | 7.6±1.1 (7.6±1.1) |
| N4222 | Sd | 31.8±0.4 | ... | ... | ... | ... | 9.9±0.2 | 4.9±0.8 (4.5±0.9) |
| N4237 | SAB(rs)bc | 31.4±0.8 | 28.5±11.5 (CFHT/u) | 4.7±2.0 | 62.0± 9.3 | 5.2±0.8 | 10.2±0.3 | 5.7±1.1 (5.5±1.2) |
| N4254 | SA(s)c | 30.9±0.3 | 23.6± 2.6 (GALEX/FUV) | 5.5±0.5 | 98.0±14.7 | 6.3±0.7 | 10.7±0.1 | 6.9±0.9 (6.8±0.9) |
| N4276 | SBC | 33.1±0.8 | 18.7± 4.3 (SDSS/g) | 6.4±0.8 | ... | ... | 10.2±0.3 | 5.5±1.1 (5.3±1.2) |
| N4293 | SB(s)0/a | 30.8±0.6 | ... | ... | 118.0±17.7 | 6.8±0.7 | 10.5±0.2 | 6.3±1.0 (6.2±1.0) |
| N4294 | SB(s)cd | 31.1±0.4 | 35.5± 2.6 (CFHT/z) | 3.5±0.6 | ... | ... | 9.7±0.2 | 4.2±0.8 (3.8±0.9) |
| N4298 | SA(rs)c | 31.0±0.3 | 23.5± 4.1 (Spitzer/IRAC2) | 5.6±0.8 | 42.0± 6.3 | 4.2±0.8 | 10.2±0.2 | 5.7±0.8 (5.4±0.9) |
| N4299 | SAB(s)dm | 31.7±0.3 | 24.6± 7.8 (CFHT/u) | 5.4±1.4 | ... | ... | 9.5±0.1 | 3.9±0.8 (3.3±0.8) |
| N4302 | Sc | 31.4±0.7 | ... | ... | ... | ... | 10.5±0.3 | 6.5±1.1 (6.4±1.2) |
| N4303 ^a | SAB(rs)bc | 30.6±0.9 | 14.7± 0.9 (GALEX/NUV) | 6.6±0.2 | 96.0±14.4 | 6.3±0.7 | 10.6±0.4 | 6.7±1.3 (6.6±1.4) |
| N4307 | Sb | 31.7±0.3 | ... | ... | ... | ... | 10.3±0.1 | 6.0±0.8 (5.7±0.9) |
| N4312 | SA(rs)ab | 30.2±0.2 | ... | ... | 69.0±10.4 | 5.4±0.7 | 9.6±0.1 | 4.1±0.7 (3.6±0.8) |
| N4313 | SA(rs)ab | 30.8±0.4 | ... | ... | 63.0± 9.5 | 5.2±0.8 | 10.0±0.2 | 5.2±0.8 (4.9±0.9) |
| N4316 | Scd? | 32.2±0.3 | ... | ... | ... | ... | 10.3±0.1 | 5.9±0.8 (5.6±0.9) |
| N4321 | AB(s)bc | 31.0±0.4 | 13.4± 3.6 (SDSS/g) | 7.3±0.7 | 91.0±13.7 | 6.1±0.7 | 10.9±0.2 | 7.6±1.2 (7.7±1.1) |
| N4330 | Scd | 31.4±0.1 | ... | ... | ... | ... | 9.9±0.1 | 4.8±0.7 (4.4±0.8) |
| N4343 | SA(rs)b | 32.1±0.3 | ... | ... | ... | ... | 10.4±0.1 | 6.1±0.8 (6.0±0.9) |
| N4356 | Scd | 31.7±0.6 | ... | ... | ... | ... | 10.0±0.3 | 5.1±1.0 (4.7±1.1) |
| N4380 | SA(rs)b | 31.4±0.4 | 20.0± 7.0 (Spitzer/IRAC4) | 6.2±1.2 | 85.0±12.8 | 6.0±0.7 | 10.3±0.2 | 5.8±0.8 (5.6±0.9) |
| N4388 ^a | SA(s)b | 31.4±0.5 | 18.6± 2.6 (KPNO 2.3m/K _s) | 6.9±0.1 | 99.0±14.9 | 6.3±0.7 | 10.5±0.2 | 6.4±0.9 (6.2±1.0) |
| N4390 | SAB(s)c | 31.6±1.0 | 21.7± 9.9 (CFHT/u) | 5.9±1.7 | ... | ... | 9.5±0.4 | 3.9±1.3 (3.4±1.5) |
| N4394 | SB(r)b | 31.2±0.3 | 10.9± 6.7 (SDSS/g) | 7.7±1.2 | 120.0±18.0 | 6.8±0.7 | 10.4±0.2 | 6.2±0.8 (6.0±0.9) |
| N4396 | SAd | 30.7±0.3 | ... | ... | ... | ... | 9.3±0.1 | 3.2±0.8 (2.6±0.8) |
| N4402 | Sb | 30.8±0.5 | ... | ... | ... | ... | 10.1±0.2 | 5.3±0.9 (5.0±1.0) |
| N4405 | SA(rs)0/a | 31.2±0.4 | ... | ... | ... | ... | 9.9±0.2 | 4.8±0.8 (4.4±0.9) |
| N4411b | SAB(s)cd | 31.7±0.8 | 23.4± 1.6 (CFHT/u) | 5.6±0.4 | ... | ... | 9.7±0.3 | 4.5±1.1 (4.0±1.2) |
| N4412 | SB(r)b | 32.8±0.8 | 10.8± 3.9 (SDSS/u) | 7.7±0.8 | ... | ... | 10.3±0.3 | 6.0±1.3 (5.8±1.2) |
| N4413 | SB(rs)ab | 31.0±0.2 | 29.8± 2.7 (GALEX/FUV & NUV) | 4.5±0.6 | ... | ... | 9.6±0.1 | 4.1±0.7 (3.6±0.8) |
| N4416 | SB(rs)cd | 33.1±0.8 | 32.0± 9.7 (SDSS/u) | 4.1±1.7 | ... | ... | 10.3±0.3 | 5.9±1.1 (5.7±1.2) |
| N4419 | SB(s)a | 31.0±0.5 | ... | ... | 102.0±15.3 | 6.4±0.7 | 10.4±0.2 | 6.3±0.9 (6.1±1.0) |
| N4424 | SB(s)a | 30.6±1.0 | 16.9± 2.4 (SDSS/r) | 6.7±0.5 | 57.0± 8.6 | 5.0±0.8 | 9.8±0.4 | 4.6±1.3 (4.2±1.5) |
| N4429 | SA0(r) | 31.0±0.6 | ... | ... | 173.0±26.0 | 7.7±0.6 | 10.8±0.2 | 7.2±1.1 (7.2±1.1) |
| N4430 | SB(rs)b | 31.2±0.9 | 20.1± 8.2 (SDSS/g) | 6.1±1.4 | ... | ... | 9.9±0.4 | 4.8±1.2 (4.4±1.4) |
| N4438 | SA(s)0/a | 30.2±0.7 | ... | ... | 135.0±20.2 | 7.1±0.7 | 10.4±0.3 | 6.3±1.0 (6.1±1.1) |
| N4445 | Sab | 31.2±0.5 | ... | ... | ... | ... | 9.7±0.2 | 4.3±0.8 (3.8±0.9) |
| N4450 | SA(s)ab | 30.8±0.5 | 10.1± 2.4 (Spitzer/IRAC4) | 7.8±0.5 | 132.0±19.8 | 7.0±0.7 | 10.7±0.2 | 6.9±1.0 (6.9±1.0) |
| N4451 | Sbc | 32.0±0.4 | ... | ... | ... | ... | 9.9±0.2 | 5.0±0.8 (4.6±0.9) |
| N4457 | SAB(s)0/a | 30.3±0.5 | ... | ... | 113.0±17.0 | 6.7±0.7 | 10.2±0.2 | 5.6±0.9 (5.3±1.0) |
| N4469 | SB(s)0/a | 31.1±0.8 | ... | ... | 106.0±15.9 | 6.5±0.7 | 10.4±0.3 | 6.1±1.1 (5.9±1.2) |
| N4470 | Sa | 31.2±0.7 | 29.2±14.9 (SDSS/gri) | 4.6±2.6 | 90.0±13.5 | 6.1±0.7 | 9.6±0.3 | 4.1±1.0 (3.6±1.1) |
| N4480 | SAB(s)c | 33.0±0.2 | 18.4± 0.9 (Spitzer/IRAC2) | 6.4±0.3 | ... | ... | 10.4±0.1 | 6.3±0.8 (6.1±0.8) |
| N4498 | SAB(s)d | 31.0±0.5 | 22.2±10.5 (GALEX/NUV) | 5.8±1.8 | ... | ... | 9.7±0.2 | 4.3±0.8 (3.8±0.9) |
| N4501 ^a | SA(rs)b | 31.2±0.5 | 12.2± 3.4 (GALEX/NUV) | 7.1±0.8 | 166.0±24.9 | 7.6±0.6 | 11.1±0.2 | 8.0±1.6 (8.2±1.4) |
| N4519 | SB(rs)d | 31.6±0.8 | 23.9±13.4 (GALEX/FUV) | 5.5±2.3 | ... | ... | 9.9±0.3 | 4.7±1.1 (4.4±1.2) |
| N4522 | SB(s)cd | 31.1±0.5 | ... | ... | ... | ... | 9.7±0.2 | 4.3±0.9 (3.8±1.0) |
| N4527 | SAB(s)bc | 30.7±0.4 | 12.8± 3.1 (Spitzer/IRAC2) | 7.4±0.6 | 135.0±20.2 | 7.1±0.7 | 10.6±0.2 | 6.8±0.9 (6.7±1.0) |
| N4532 | IBm | 30.6±0.5 | ... | ... | ... | ... | 9.6±0.2 | 4.0±0.9 (3.5±1.0) |
| N4535 | SAB(s)c | 30.9±0.5 | 21.9± 4.0 (Spitzer/IRAC2) | 5.8±0.8 | 102.0±15.3 | 6.4±0.7 | 10.6±0.2 | 6.7±1.0 (6.6±1.0) |
| N4536 | SAB(rs)bc | 30.9±0.4 | 20.2± 2.3 (Spitzer/IRAC2) | 6.1±0.5 | 111.0±16.7 | 6.6±0.7 | 10.4±0.2 | 6.3±0.9 (6.1±0.9) |
| N4548 | SB(rs)b | 31.0±0.3 | 14.6± 3.6 (SDSS/u) | 7.1±0.7 | 122.0±18.3 | 6.8±0.7 | 10.7±0.2 | 6.9±0.9 (6.8±0.9) |
| N4567 | SA(rs)bc | 31.8±0.5 | 13.4± 1.4 (SDSS/g) | 7.3±0.4 | 66.0± 9.9 | 5.3±0.7 | 10.5±0.2 | 6.4±0.9 (6.3±1.0) |
| N4568 | SA(rs)bc | 31.5±0.6 | 21.7± 5.2 (Spitzer/IRAC1) | 5.9±0.9 | 88.0±13.2 | 6.0±0.7 | 10.7±0.2 | 7.0±1.1 (7.0±1.1) |
| N4569 | SAB(rs)ab | 30.4±0.6 | 14.3± 6.8 (SDSS/g) | 7.1±1.2 | 139.0±20.9 | 7.2±0.7 | 10.6±0.2 | 6.8±1.0 (6.7±1.1) |
| N4571 | SA(r)d | 31.0±0.3 | 11.2± 7.4 (HST/F555W) | 7.7±1.3 | ... | ... | 10.1±0.1 | 5.5±0.8 (5.2±0.8) |

Table A2. Continued.

| Galaxy | Type | Dist.Mod. | $ \phi $ (band) [deg] | $\log M_{\text{bh}}(\phi)$ [dex] | σ km s ⁻¹ | $\log M_{\text{bh}}(\sigma)$ [dex] | $\log M_{*,\text{gal}}$ [dex] | $\log M_{\text{bh}}(M_{*,\text{gal}})$ [dex] |
|--------|-----------|-----------|----------------------------|---------------------------------------|--------------------------------|---------------------------------------|----------------------------------|---|
| N4579 | SAB(rs)b | 31.3±0.4 | 6.1± 3.9 (Spitzer/IRAC4) | 8.5±0.8 | 166.0±24.9 | 7.6±0.6 | 11.1±0.2 | 7.9±1.4 (8.0±1.3) |
| N4580 | SAB(rs)a | 31.4±1.1 | 20.2± 6.2 (SDSS/griz) | 6.1±1.1 | ... | ... | 10.1±0.4 | 5.4±1.3 (5.1±1.5) |
| N4606 | SB(s)a | 31.0±0.5 | ... | ... | ... | ... | 9.8±0.2 | 4.5±0.9 (4.0±1.0) |
| N4607 | SBb? | 31.0±0.9 | ... | ... | ... | ... | 9.7±0.4 | 4.4±1.2 (4.0±1.3) |
| N4639 | SAB(rs)bc | 31.8±0.2 | 17.5± 4.9 (SDSS/g) | 6.6±0.9 | 91.0±13.7 | 6.1±0.7 | 10.3±0.1 | 6.0±0.8 (5.8±0.8) |
| N4647 | SAB(rs)c | 31.2±0.3 | 21.4± 2.6 (Spitzer/IRAC2) | 5.9±0.5 | 49.0± 7.4 | 4.6±0.8 | 10.2±0.2 | 5.6±0.8 (5.3±0.9) |
| N4651 | SA(rs)c | 31.7±0.8 | 14.3± 1.0 (CFHT/u) | 7.1±0.4 | 101.0±15.2 | 6.4±0.7 | 10.6±0.3 | 6.7±1.1 (6.6±1.3) |
| N4654 | SAB(rs)cd | 30.8±0.5 | 25.5± 9.3 (Spitzer/IRAC3) | 5.2±1.6 | 48.0± 7.2 | 4.6±0.8 | 10.4±0.2 | 6.1±0.9 (5.9±1.0) |
| N4689 | SA(rs)bc | 31.0±0.4 | 24.1± 7.2 (Spitzer/IRAC2) | 5.4±1.3 | 41.0± 6.2 | 4.2±0.8 | 10.1±0.2 | 5.5±0.8 (5.2±0.9) |
| N4698 | SA(s)ab | 31.6±0.8 | ... | ... | 137.0±20.6 | 7.1±0.7 | 10.8±0.3 | 7.1±1.2 (7.1±1.3) |
| N4713 | SAB(rs)d | 30.6±0.8 | 35.4±10.8 (HST F606W) | 3.5±1.9 | 23.0± 3.5 | 2.8±1.0 | 9.6±0.3 | 4.0±1.1 (3.5±1.2) |

^a Directly measured black hole masses exist for these three galaxies (see Section 2). The galaxy and black hole masses in this table are in units of solar masses. The three sets of predicted black hole mass are based on: the spiral arm's pitch angle ϕ using equation 2; the galaxy's central velocity dispersion σ using equation 3; and the galaxy's stellar mass $M_{*,\text{galaxy}}$ derived using equation 4 (and equation 5).